

**A COMPLIANT SUSPENSION APPLICATION TO A SMALL
SCALE CAR**

**KÜÇÜK ÖLÇEKLİ BİR OTOMOBİLE ESNEK
SÜSPANSİYON UYGULAMASI**

ÇAĞRI BEKİR BAYSAL

PROF. DR ENGİN TANIK
Supervisor

Submitted to
Graduate School of Science and Engineering of Hacettepe University
as a Fulfillment to the Requirements
for the Award of the Degree of Master of Science
in Mechanical Engineering.

2019

This work titled **A COMPLIANT SUSPENSION APPLICATION TO A SMALL SCALE CAR**” by **ÇAĞRI BEKİR BAYSAL** has been approved as a thesis for the degree of Master of Science in Mechanical Engineering by the Examining Committee Members mentioned below.

Doç. Dr. Volkan Parlaktaş

Head



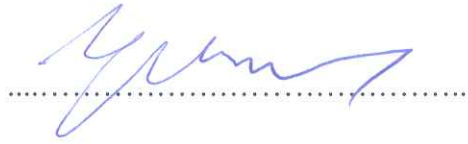
Prof. Dr. Engin Tanık

Supervisor



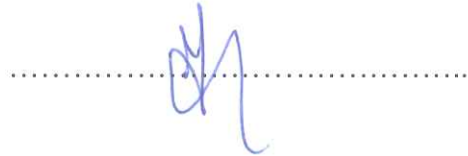
Doç. Dr. Tuncay Karaçay

Member



Doç. Dr. Yiğit Karpaz

Member



Doç. Dr. Barış Sabuncuoğlu

Member



This thesis has been approved as a thesis for the degree of Master of Science in Mechanical Engineering by Board of Directors of the Institute of Graduate School of Science and Engineering on / /.....

Prof. Dr. Menemşe GÜMÜŞDERELİOĞLU
Director of the Institute of
Graduate School of Science and Engineering

ETİK

Hacettepe Üniversitesi Fen Bilimleri Enstitüsü, tez yazım kurallarına uygun olarak hazırladığım bu tez çalışmada,

- tez içindeki bütün bilgi ve belgeleri akademik kurallar çerçevesinde elde ettiğimi,
- görsel, işitsel ve yazılı tüm bilgi ve sonuçları bilimsel ahlak kurallarına uygun olarak sunduğumu,
- başkalarının eserlerinden yararlanılması durumunda ilgili eserlere bilimsel normlara uygun olarak atıfta bulunduğumu,
- atıfta bulunduğum eserlerin tümünü kaynak olarak gösterdiğimi,
- kullanılan verilerde herhangi bir değişiklik yapmadığımı,
- ve bu tezin herhangi bir bölümünü bu üniversite veya başka bir üniversitede başka bir tez çalışması olarak sunmadığımı

beyan ederim.

18 / 02 / 2019



Çağrı Bekir Baysal

YAYINLANMA FİKRİ MÜLKİYET HAKKLARI BEYANI

Enstitü tarafından onaylanan lisansüstü tezimin/raporumun tamamını veya herhangi bir kısmını, basılı (kağıt) ve elektronik formatta arşivleme ve aşağıda verilen koşullarla kullanıma açma iznini Hacettepe üniversitesine verdiğimi bildiririm. Bu izinle Üniversiteye verilen kullanım hakları dışındaki tüm fikri mülkiyet haklarım bende kalacak, tezimin tamamının ya da bir bölümünün gelecekteki çalışmalarda (makale, kitap, lisans ve patent vb.) kullanım hakları bana ait olacaktır.

Tezin kendi orijinal çalışmam olduğunu, başkalarının haklarını ihlal etmediğimi ve tezimin tek yetkili sahibi olduğumu beyan ve taahhüt ederim. Tezimde yer alan telif hakkı bulunan ve sahiplerinden yazılı izin alınarak kullanması zorunlu metinlerin yazılı izin alarak kullandığımı ve istenildiğinde suretlerini Üniversiteye teslim etmeyi taahhüt ederim.

Yükseköğretim Kurulu tarafından yayınlanan “*Lisansüstü Tezlerin Elektronik Ortamda Toplanması, Düzenlenmesi ve Erişime Açılmasına İlişkin Yönerge*” kapsamında tezimin aşağıda belirtilen koşullar haricince YÖK Ulusal Tez Merkezi / H. Ü. Kütüphaneleri Açık Erişim Sisteminde erişime açılır.

- Enstitü / Fakülte yönetim kurulu kararı ile tezimin erişime açılması mezuniyet tarihimden itibaren 2 yıl ertelenmiştir.
- Enstitü / Fakülte yönetim kurulu gerekçeli kararı ile tezimin erişime açılması mezuniyet tarihimden itibaren ay ertelenmiştir.
- Tezim ile ilgili gizlilik kararı verilmiştir.

18 / 02 / 2019



Çağrı Bekir Baysal

ÖZET

KÜÇÜK ÖLÇEKLİ BİR OTOMOBİL İÇİN ESNEK SÜSPANSİYON UYGULAMASI

Çağrı Bekir Baysal

Yüksek Lisans, Makina Mühendisliği Bölümü

Tez Danışmanı: Prof. Dr. Engin TANIK

Ocak 2019, 50 Sayfa

Sunulan tez kapsamında çift salıncaklı bir süspansiyon mekanizmasına esnek mekanizma alternatifinin eşdeğerliği değerlendirilmiştir. Referans rijit çift salıncak süspansiyon mekanizması küçük ölçekli bir model araçtan alınmıştır. Model olarak kullanılan süspansiyon, aracın sol arka süspansiyon mekanizmasıdır.

Referans süspansiyon mekanizması CATIA yazılımı kullanılarak modellenmiştir. Bu 3D model, gerekli pozisyon ve ölçüleri elde etmek için kullanılmıştır. Referans süspansiyon mekanizmasına kinematik analiz yapıldıktan sonra bir ara basamak olarak daha küçük boyutlarda eşdeğer bir rijit mekanizma tasarımı yapılması gerekmektedir. Eşdeğer rijit mekanizma referans mekanizma ile aynı kamber, kaster ve rot açıları değişimi gibi kinematik özelliklere sahip olacak şekilde tasarlanmıştır. Bu ara basamak, referans süspansiyon mekanizması doğrudan esnek mekanizmaya dönüştürülemeyeceği için gerekmektedir. Bunun sebebi, bir rijit mekanizma sahte-rijit-cisim metodu ile esnek alternatifine dönüştürüldüğünde ulaşılan esnek mekanizmanın boyutunun rijit versiyonundan büyük olmasıdır. Bu bağlamda ara basamak olarak tasarlanan eşdeğer rijit mekanizma esnek alternatifine dönüştürüldüğünde referans süspansiyon mekanizması ile aynı kinematik özelliklere sahip olmaktadır ve araç üzerinde aynı hacme monte edilebilecektir.

Salıncak mafsallarında sabit kılavuzlu mafsal yaklaşımı kullanılarak esnek mekanizma alternatifi oluşturulmuştur. Ön analizler sonrasında esnek salıncak mafsallarında yüksek gerilim değerleri olduğu gözlemlenmiştir ve bu değerlerin düşürülmesi gerekmiştir. Bu

sorun, esnek alt salıncak mafsalında çift katman kullanma yaklaşımı ile çözülmüştür. Yaklaşım ile esnek mafsal eşdeğer mesnetlerinin konumu bozulmadan üzerindeki gerilimler azaltılmıştır. Bu yaklaşım literatürde bulunmamaktadır.

Sonlu elemanlar analizi ANSYS yazılımı ile gerçekleştirilmiştir. Analizler statik yük, maksimum süspansiyon yükü, maksimum frenleme ve kaldırma çarpma senaryoları için gerçekleştirilmiştir. Sonlu elemanlar analizi ile analitik yaklaşımın yetkinliği kontrol edilip, nihai esnek mekanizma tasarımının referans süspansiyon mekanizmasına eşdeğerliği kanıtlanmıştır.

Anahtar Kelimeler: esnek mekanizmalar, rijit mekanizmalar, çift salıncak süspansiyon, sonlu elemanlar metodu, sahte-rijit-cisim metodu

ABSTRACT

A COMPLIANT SUSPENSION APPLICATION TO A SMALL SCALE CAR

Çağrı Bekir Baysal

Master of Science, Department of Mechanical Engineering

Supervisor: Prof. Dr. Engin TANIK

January 2019, 50 Pages

Compatibility of a compliant equivalent for a double wishbone suspension is assessed in this thesis. Reference rigid double wishbone suspension is taken from a small-scale model car. Rear left suspension of this model car is used as a reference to compare the compliant mechanism.

Reference suspension mechanism is modeled using CATIA software. This 3D model is used for obtaining necessary dimensions and positions for kinematic analysis. After conducting the kinematic analysis of the reference suspension mechanism, a smaller equivalent rigid link mechanism needs to be designed as a sub step. The equivalent rigid link mechanism is designed to have the same kinematic properties such as camber, caster, toe variation etc. This sub step is performed because we cannot convert the reference suspension mechanism directly to its compliant equivalent. The reason for that is using pseudo rigid body method to convert a rigid link mechanism results in a bigger compliant equivalent than the mechanism itself. Therefore, converting the smaller rigid link equivalent mechanism to its compliant equivalent will result in a mechanism which has the same kinematic properties as the reference suspension mechanism and can be mounted in the same space on the vehicle. Compliant equivalent design was performed using fixed guided beams as compliant wishbone sections. After completing initial analyses, stress values on the compliant sections needed to be reduced. This is performed by introducing a novel approach by transforming

the compliant lower wishbone to double layer formation. This approach keeps the pseudo joints of the compliant link and reduces the stress at the same time.

Finite element analyses of the mechanism are performed on ANSYS software. Analyses are performed for static loading, maximum bump loading, maximum braking and curb hitting scenarios. Analytical approach is checked with finite element analysis and final compliant design is proven as an equivalent for the reference suspension mechanism.

Keywords: compliant mechanisms, rigid link mechanisms, double wishbone suspension, finite elements method, pseudo rigid body method



TEŐEKKÜR

Lisans ve yüksek lisans eđitimim boyunca ilgi ve desteđini esirgemeyen, tez alıőmamın her aőamasında da büyük emeđi olan tez danıőmanım Prof. Dr. Engin TANIK'a,

Sonlu elemanlar analiz metodu konusunda vakit ayırarak karőılaőtım sorunları özmeme yardımcı olan Merve TANIK'a,

Hayatım boyunca her koőulda desteđini esirgemeyen ve yanımda olan, emeđini ödeyemeyeceđim canım aileme,

Sonsuz Teőekkürler,

ađrı Bekir Baysal
Őubat 2019, Ankara

CONTENTS

ÖZET	i
ABSTRACT	iii
TEŞEKKÜR	v
LIST OF FIGURES	vii
LIST OF TABLES	ix
1. INTRODUCTION	1
2. LITERATURE SURVEY	2
2.1. Mechanisms	2
2.1.1. Conventional Rigid Link Mechanisms	2
2.1.2. Compliant Mechanisms	7
3. METHODOLOGY	14
3.1. Suspension Analysis Method	16
3.2. Rigid Body Suspension Analysis	22
3.3. Construction of Rigid Body Equivalent of the Desired Compliant Mechanism ..	25
3.4. Equivalent Spring Rate Calculation of the Compliant Suspension	28
3.5. A Novel Approach to Increase Stiffness of the Compliant Suspension Mechanism	32
3.6. Design of the Compliant Mechanism by using Rigid Body Replacement Technique	33
3.7. Verification of the Compliant Mechanism via Finite Element Analysis	34
3.7.1. Static Loading Scenario	37
3.7.2. Maximum Bump Loading Scenario	38
3.7.3. Maximum Braking Scenario	40
3.7.4. Curb Hitting Scenario	43
4. CONCLUSION	48
5. REFERENCES	49

LIST OF FIGURES

Figure 1 A Four Bar Mechanism	3
Figure 2 Simple Representation of a Double Wishbone Suspension [2]	4
Figure 3 Double Wishbone Suspension [5].....	4
Figure 4 Visual Representation of Camber Angle [8]	5
Figure 5 Kingpin (a) and Caster (b) Angles	6
Figure 6 Toe Angle [8].....	6
Figure 7 A Partially Compliant Mechanism.....	8
Figure 8 Allred and Howell Compliant A-Arm.....	10
Figure 9 Compliant Suspension Mechanism (Allred and Howell).....	10
Figure 10 Steel Compliant Cardan Universal Joint (Merve Tank et al.)	11
Figure 11 Chevrolet Corvette Suspension System with Leaf Spring	12
Figure 12 Fixed Free Compliant Beam and Rigid Body Equivalent [11].....	12
Figure 13 Small Length Flexural Pivot and Rigid Body Equivalent [11].....	13
Figure 14 Compliant Four Bar Mechanism and Rigid Body Equivalent [11]	13
Figure 15 Scale Car Rigid Link Suspension 3D Model.....	14
Figure 16 Scale Car Rigid Body Suspension	15
Figure 17 Double Wishbone Suspension Mechanism Parameters [5].....	16
Figure 18 Vector Transformations.....	20
Figure 19 Camber, Caster, Kingpin and Toe Angle Measurement [5].....	22
Figure 20 Rigid Link Mechanism Camber Variation	23
Figure 21 Rigid Link Mechanism Caster Variation.....	24
Figure 22 Rigid Link Mechanism Kingpin Variation.....	24
Figure 23 Rigid Link Mechanism Half Track Variation.....	24
Figure 24 Rigid Link Mechanism Toe Variation	25
Figure 25 Rigid Body Equivalent and Desired Compliant Mechanism.....	25
Figure 26 Equivalent Rigid Link Mechanism Camber Variation.....	27
Figure 27 Equivalent Rigid Link Mechanism Caster Variation	27
Figure 28 Equivalent Rigid Link Mechanism Kingpin Variation	27
Figure 29 Equivalent Rigid Link Mechanism Half Track Variation	28
Figure 30 Equivalent Rigid Link Mechanism Toe Variation.....	28
Figure 31 Simplified Expression for the 2D Mechanism Undeformed Position	29

Figure 32 Equivalent Spring Constant Parameters	31
Figure 33 3D Model of the Compliant Mechanism	33
Figure 34 Single-Double Layer Compliant Mechanism and Rigid Link Equivalent.....	33
Figure 35 Holder Geometry	35
Figure 36 Analysis Model Meshing	36
Figure 37 Compliant Section Meshes.....	36
Figure 38 Analysis Project Tree and Commands	37
Figure 39 Static Loading Scenario, Deformation.....	37
Figure 40 Static Loading Scenario, Von-Mises Stress	38
Figure 41 Maximum Bump Loading Scenario, Deformation	39
Figure 42 Maximum Bump Loading Scenario, Von-Mises Stress	39
Figure 43 Maximum Braking Scenario	40
Figure 44 Maximum Braking Scenario Force (a) Moment (b) Plot.....	41
Figure 45 Maximum Braking Scenario, Deformation.....	42
Figure 46 Maximum Braking Scenario, Von-Mises Stress	42
Figure 47 Maximum Braking Scenario, X Axis Directional Deformation	43
Figure 48 Curb Hitting Scenario	43
Figure 49 Curb Hitting Scenario Force (a) Moment (b) Plot.....	44
Figure 50 Curb Hitting Scenario, Deformation.....	45
Figure 51 Curb Hitting Scenario, Von-Mises Stress	45

LIST OF TABLES

Table 1 Yield strength / Young's Modulus Ratio and Resilience	9
Table 2 Suspension Components' Weights	15
Table 3 Suspension Analysis Variables	17
Table 4 Suspension Analysis Parameters	23
Table 5 Parameters of the Rigid Link Equivalent of Compliant Mechanism	26
Table 6 Compliant Mechanism Parameters	34
Table 7 Material Properties of Blue Polished Steel	35
Table 8 FEA and Calculation Deflection Comparison Table	47
Table 9 FEA and Calculation Von Misses Stress Comparison Table	47
Table 10 FEA and Calculation Camber Comparison Table	47

1. INTRODUCTION

Aim of this thesis is to assess the compatibility of a compliant mechanism as an equivalent of a four-bar double wishbone suspension mechanism. A small-scale model car is used as a reference to design the equivalent compliant mechanism.

From the main dimensions of this suspension, 3D model of it is created using CATIA software. Having the model on a CAD software is helpful at the kinematic analysis stage because 3D model will be used to get every necessary position and length data for every link. After completing the kinematic analysis stage, a design procedure for the equivalent rigid body mechanism is proposed. A smaller equivalent rigid body mechanism is synthesized to be used because after converting this mechanism to a compliant version using pseudo rigid body replacement method, compliant version will be bigger in size due to the nature of this method. While converting the equivalent rigid link mechanism to compliant mechanism, multiple iterations are used to get desired stress values and rigidity.

After completing the compliant mechanism design using rigid body replacement method, the mechanism is analyzed using ANSYS. Different scenarios like; braking, curb hitting, static load, and bump load cases are analyzed with ANSYS.

By using results of the FEM analysis, calculations obtained from analytical approach are compared. Finally, feasibility of the design procedure given in this thesis to design an equivalent compliant mechanism is discussed.

2. LITERATURE SURVEY

2.1. Mechanisms

Reuleaux defines the conventional rigid mechanism as an ‘assemblage of resistant bodies, connected by movable joints, to form a closed kinematic chain with one link fixed and having the purpose of transforming motion. A kinematic chain consists of links which are connected by kinematic pairs [1]. Mechanisms transmit motion through their links and can be used to make monotonous tasks repeatedly [2].

Mechanisms can be divided into two groups with their link types; rigid link mechanisms and compliant mechanisms. A rigid link mechanism only consists of rigid links and joints. On the other hand, compliant mechanisms have at least one compliant segment and may or may not have joints [3].

Output of a mechanism can be either proportional to the input or it can be nonlinear with respect to the input. Mechanisms are designed to provide desired output with both position and transmission ratio. If all links of a mechanism moves on the same plane, it is called planar mechanism. If one or more links of the mechanism move on non-parallel planes, it is mechanism is called spatial mechanism [4].

2.1.1. Conventional Rigid Link Mechanisms

Rigid link mechanisms have links which are assumed to have no or negligible deflection. Rigid link mechanisms can have specific names depending on their link numbers, joint types etc... Some of these are four bar mechanism, slider crank mechanism, gear mechanisms etc...

One of the simplest closed loop mechanisms is the four-bar mechanism. The four-bar mechanism has one fixed and three moving links. These types of mechanisms can have revolute or spherical joints depending on output motion requirements. Planar four bar mechanisms have four revolute joints, spatial four bar mechanisms have at least two spherical joints to transmit out of plane motion.

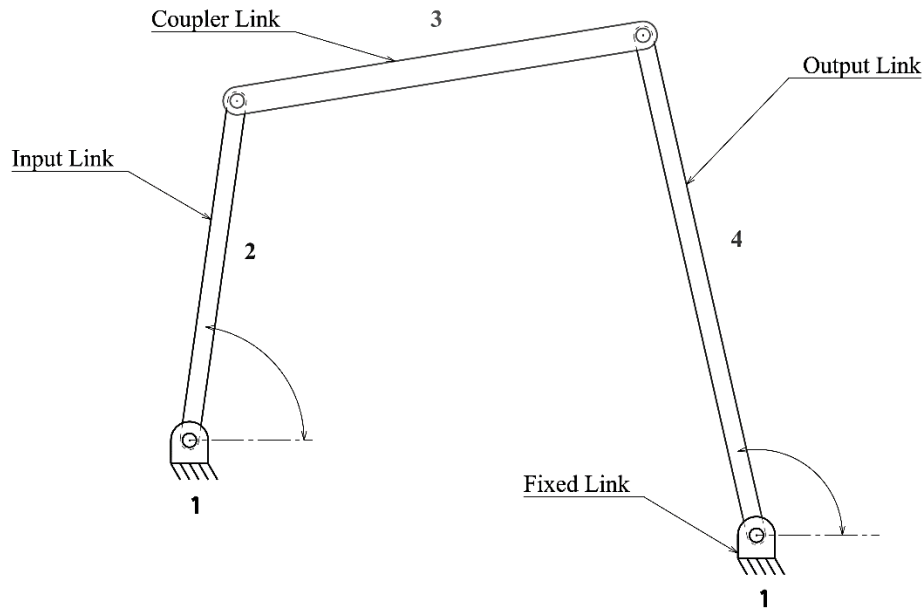


Figure 1 A Four Bar Mechanism

An example of a four-bar mechanism can be seen in Figure 1. Link 1 is ground or fixed link, links numbered 2, 3, and 4 are moving links. Link lengths and joint positions determine the path traced by the point P . These parameters are used to design the mechanism.

2.1.1.1. Double Wishbone Suspension

A simplified representation of a double wishbone car suspension is presented in Figure 2. The front double wishbone suspensions are generally spatial four bar mechanisms since an extra freedom for steering action is required. For the rear suspensions, there is generally no steering function. However, it is desired to have a small toe angle variation to achieve stability while the vehicle is moving. Because of this, these mechanisms are generally not planar and there must be an extra freedom. This freedom is provided by using spherical joints on both sides of link 3 instead of revolute joints in Figure 2.

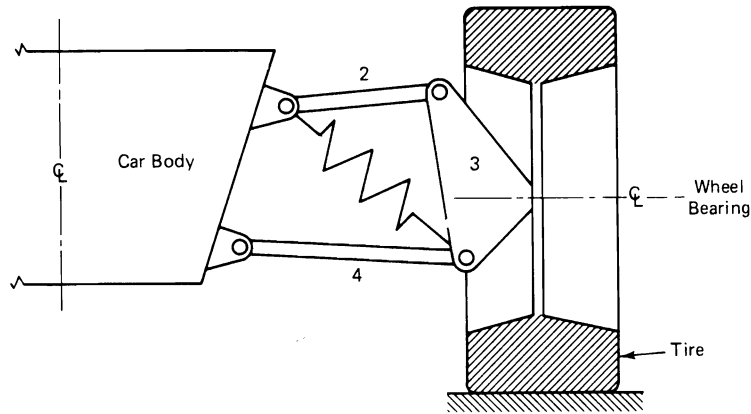


Figure 2 Simple Representation of a Double Wishbone Suspension [2]

Another reason why spatial four bar mechanisms are used over planar ones on double wishbone suspensions is that links (wishbones and knuckle) of the suspension are typically not on the same plane to satisfy with vehicle handling requirements. Even if it is a rear suspension, through the stroke of the suspension, angle of the wheel around steering axis changes and there should be freedom to be able to make wheel alignments. An example of a spatial four bar suspension mechanism is presented in Figure 3.

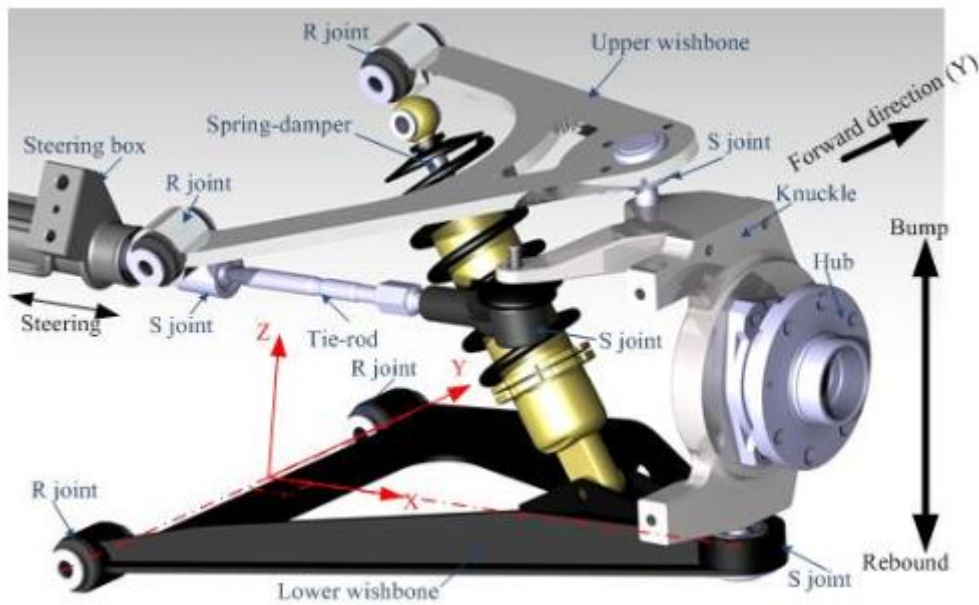


Figure 3 Double Wishbone Suspension [5]

Low weight and no mutual wheel influence characteristics are easily achieved with double wishbone suspensions [6].

Some of the primary functions of suspension systems can be listed as [7]:

- Isolate the chassis from the road surface and provide vertical compliance to the wheels.
- React to the lateral and longitudinal forces generated by the friction.
- Keeps the wheels in desired kinematic angles.
- Supports the weight of the vehicle and resists roll.

2.1.1.2. Suspension Mechanism Geometry

Suspension mechanism motions need to track some specific curves in order to satisfy a good handling and road holding. The motion curves are; camber angle, caster angle, kingpin angle, toe angle, and half-track variation.

Camber angle is the angle between vertical axis of the vehicle and wheel plane when viewed from front. The camber angle is presented in Figure 4.

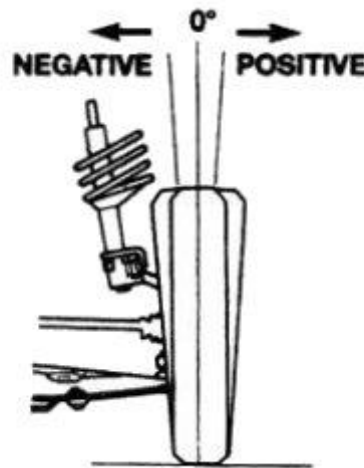


Figure 4 Visual Representation of Camber Angle [8]

Kingpin (inclination) angle is the angle between steering axis and vertical axis of a vehicle when viewed from front. Caster angle is the angle between steering axis and vertical axis of a vehicle viewed from the side. Kingpin angle and caster angle is presented in Figure 5a and Figure 5b respectively.

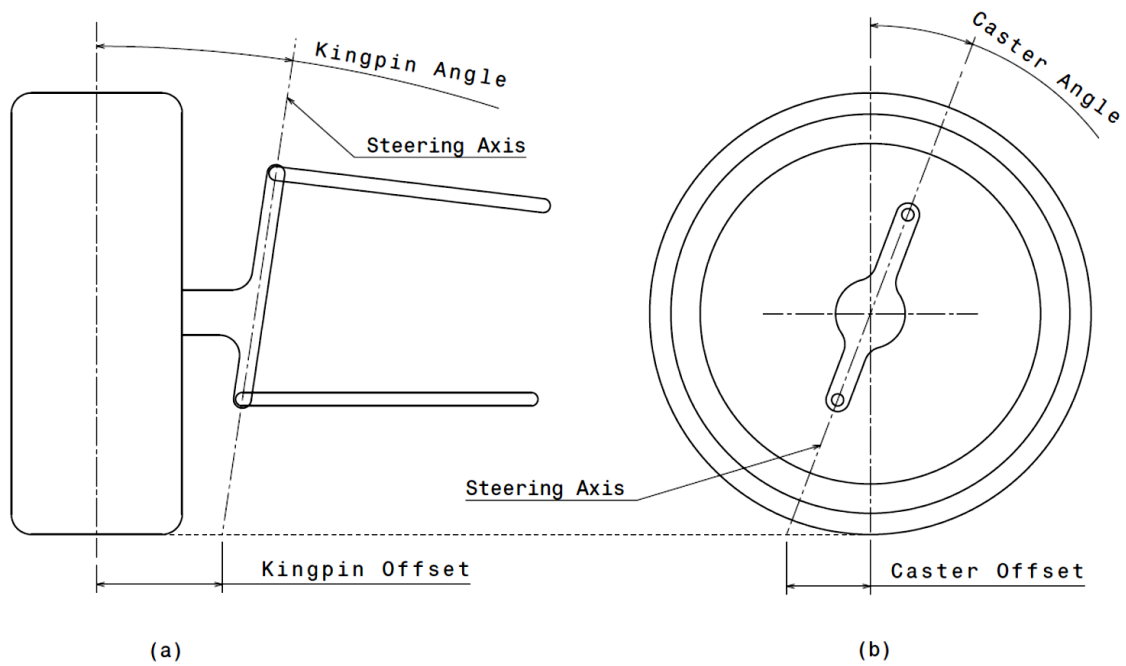


Figure 5 Kingpin (a) and Caster (b) Angles

Toe angle is the angle between wheel plane and centerline of a vehicle viewed from the top. Toe angle is presented in Figure 6.

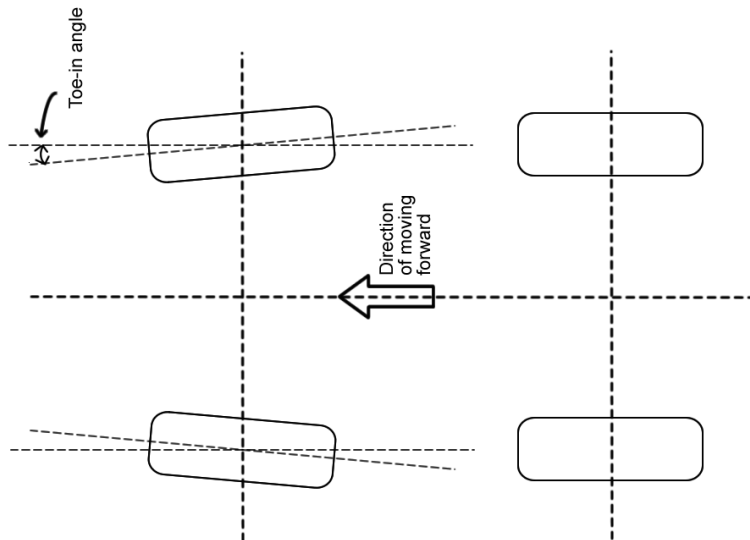


Figure 6 Toe Angle [8]

Half-track variation is the change of distance from the wheel and the centerline of the vehicle viewed from the top.

2.1.2. Compliant Mechanisms

Compliant mechanisms achieve their design goal with deflection of flexible members. This stores energy in the system to be used and this can be used in designer's favor. For example, instead of adding a spring to a mechanism, we can set the equivalent spring coefficient of the compliant section and reduce the part count, eliminate mechanical coupling reduce weight and cost. Using an equivalent compliant mechanism instead of a rigid link mechanism reduces unsprung mass and this helps the suspension system to better follow the road contour [9]. Compliant mechanisms have many advantages as described earlier however they also have some disadvantages. To design a compliant mechanism, we should first design the rigid mechanism and create the equivalent compliant mechanism by using pseudo rigid body model. This makes the design process harder and longer. Another disadvantage is whereas finite element analysis of rigid mechanisms is usually simpler and require less processing power since we usually neglect deflection, compliant mechanisms in the other hand require non-linear analysis that causes difficulty. Compliant mechanisms are being used from the past. One of the earlier examples is the bow. When the arrow is drawn, the compliant segment deflects elastically therefore stores energy. Finally, the arrow is shot with the aid of this energy.

Compliant mechanisms have at least one deflecting link while moving. Compliant mechanisms are categorized as fully or partially compliant.

The mechanism presented in Figure 7 is a partially compliant slider crank mechanism. The mechanism is an RSSP configuration and there are two compliant and two conventional joints [10].

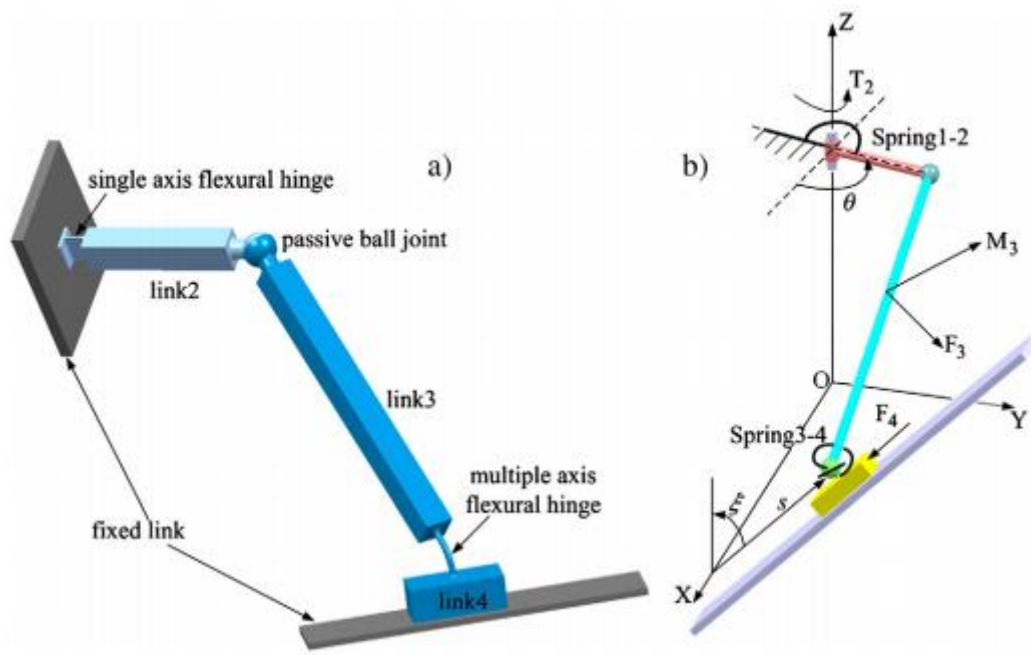


Figure 7 A Partially Compliant Mechanism

Fully compliant mechanisms have no joints and employ flexible joints to achieve the desired motion. Partially compliant mechanisms have flexible links as in fully compliant mechanisms, but they have at least one joint [11]. Compliant cardan joint mechanism presented in Figure 10 is an example of fully compliant mechanism.

Compliant mechanisms have fewer mechanical joints by their nature. Because of that, compliant equivalent of a mechanism is usually lighter. This also reduces the assembly time and cost of the mechanism. Another result of having a smaller number of joints is not having the backlash caused by mechanically connected joints. Compliant joints store energy as they deflect, this can be used as an advantage to remove the need of a spring or can be a disadvantage [4].

Compliant mechanisms have a lot of advantages, however they also have a couple of disadvantages. Design and analysis of compliant mechanisms are much more challenging than the rigid ones. Fatigue life is usually less than rigid link mechanisms. Compliant mechanisms are hard to analyze on FEM programs because explicit analyses like the ones including deflection require significantly more processing power [4].

Stiffness and strength are two different things and they shouldn't be confused with. Stiffness is the resistance to deflection on the other hand strength is related to resistance to failure. Something may be desired to be both strong and stiff like the floor of a building because it should carry the weight of everything above it and it shouldn't deflect much. In other cases,

it may need to be strong and not stiff like a pulley cable which needs to withhold the load it is carrying and needs to bend around the pulley. [11].

For compliant mechanisms, it is desired for a link to be both strong and flexible. That's why materials with high strength and low young's modulus are usually more suitable to be used as compliant. There are two similar approaches to assess a material if it is suitable to use in a compliant mechanism. First one is to check the ratio of strength to Young's modulus, higher values are desired. Second one is to check the resilience of the material. Resilience measures the amount of energy per unit volume the material can withstand without yielding [11]. Yield strength over Young's modulus ratio and resilience values of some materials are presented in Table 1.

Table 1 Yield strength / Young's Modulus Ratio and Resilience

Material	E (GPa)	S_y (MPa)	$(S_y/E) \times 1000$	$(0.5 \times S_y^2/E) \times 0.001$
Steel (1010 hot rolled)	207	179	0.87	77
Steel (4140 Q&T @400)	207	1641	7.9	6500
Aluminum (110 annealed)	71.7	34	0.48	8.1
Aluminum (7075 heat treated)	71.7	503	7.0	1800
Titanium (Ti-35A annealed)	114	207	1.8	190
Titanium (Ti-13 heat treated)	114	1170	10	6000
Nitinol (high-temperature phase)	75	560	7.5	2100
Beryllium copper (CA170)	128	1170	9.2	5300
Polycrystalline silicon	169	930	5.5	2600
Polyethylene (HDPE)	1.4	28	20	280
Nylon (type 66)	2.8	55	20	540
Polypropylene	1.4	34	25	410
Kevlar (82 vol%) in epoxy	86	1517	18	13 000
E-glass (73.3 vol%) in epoxy	56	1640	29	24 000

An example of a compliant suspension mechanism with a different approach than this thesis is the work of Timothy Allred and his advisor Larry Howell [12]. Their approach on the compliant suspension links consists of compliant A-arms. They achieved this design by approaching the A-arms as they had two compliant links in triangular formation as it is presented in Figure 8. This design adds complexity to the mathematical model of the compliant mechanism and total spring rate of the compliant mechanism will be non-linear.

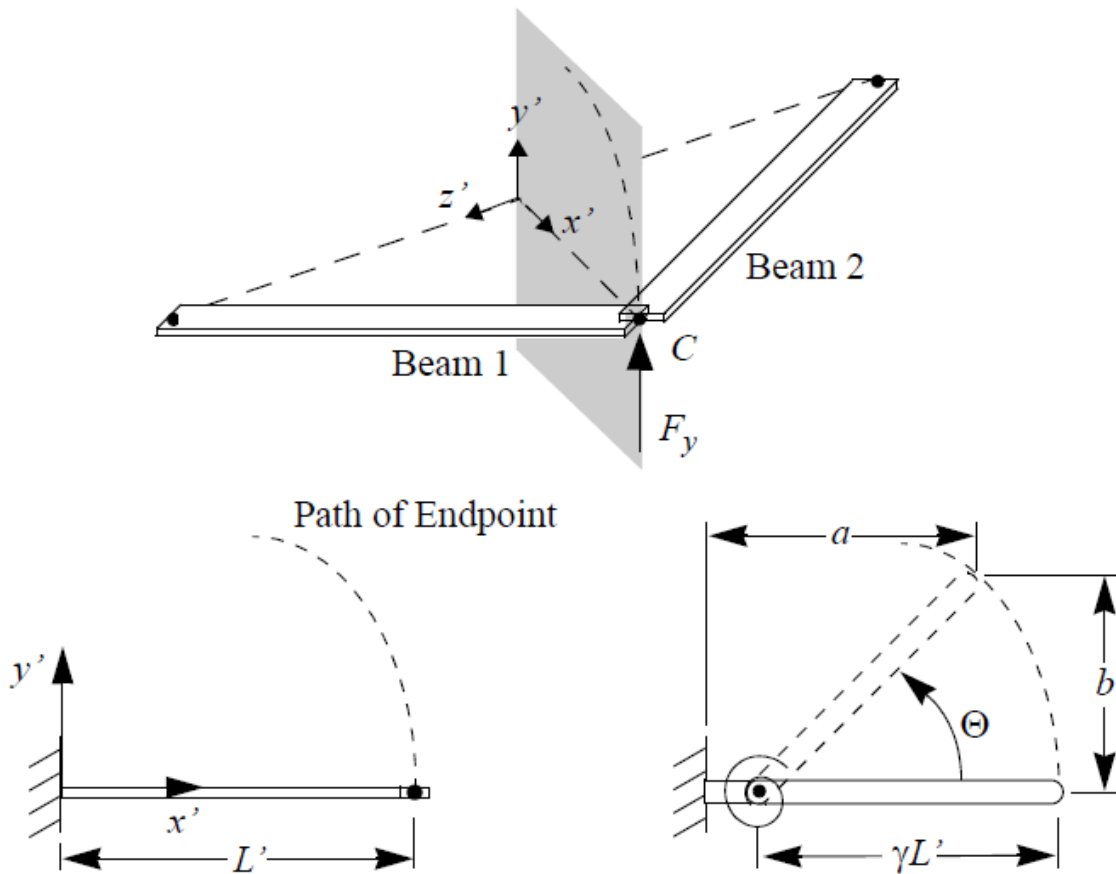


Figure 8 Allred and Howell Compliant A-Arm

Final design achieved by this approach has double A-arms in parallel formation and connections between compliant links and rigid knuckle is with a conventional revolute joint. The mechanism is presented in Figure 9.

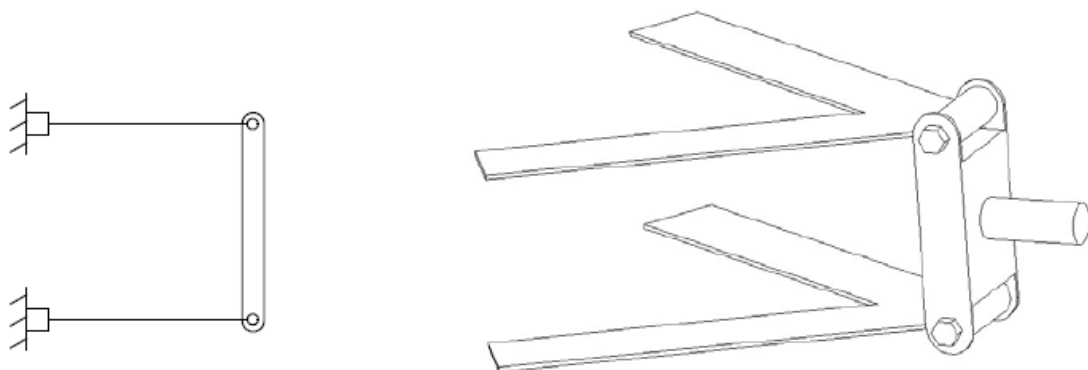


Figure 9 Compliant Suspension Mechanism (Allred and Howell)

Another example of a compliant mechanism is the steel compliant cardan universal joint [13]. This mechanism utilizes fixed free compliant sections to create a universal joint. The joint presented in Figure 10 is a fully compliant mechanism.

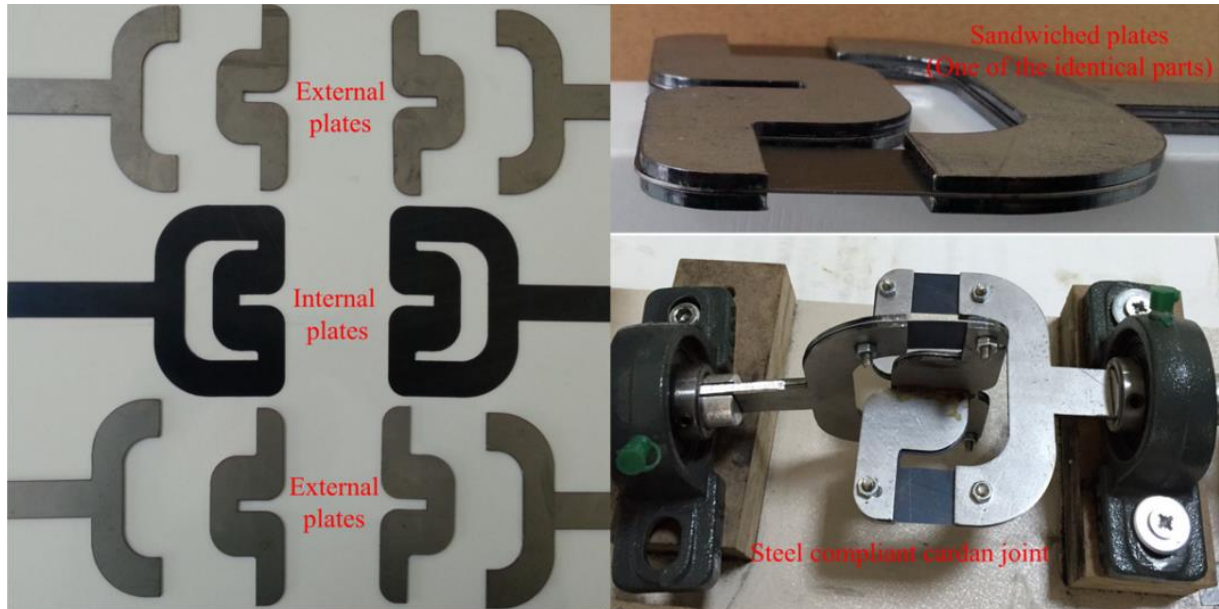


Figure 10 Steel Compliant Cardan Universal Joint (Merve Tanık et al.)

The joint is created by putting the internal plates between external plates and internal plates act as compliant sections.

This cardan joint is a good example of the utilization of compliancy in low load applications. Normally, a universal joint would require some sort of bushing or bearing because they work under high torque and speed values. For the compliant equivalent, because the torque distribution is made through compliant sections, there is no friction and the need for a joint is eliminated.

Leaf springs have been used in some vehicles' suspension systems in the past instead of coil springs. An example of this is 1997 Corvette (presented in Figure 11). This vehicle has double wishbone suspension system and uses leaf spring in order to save space [14].

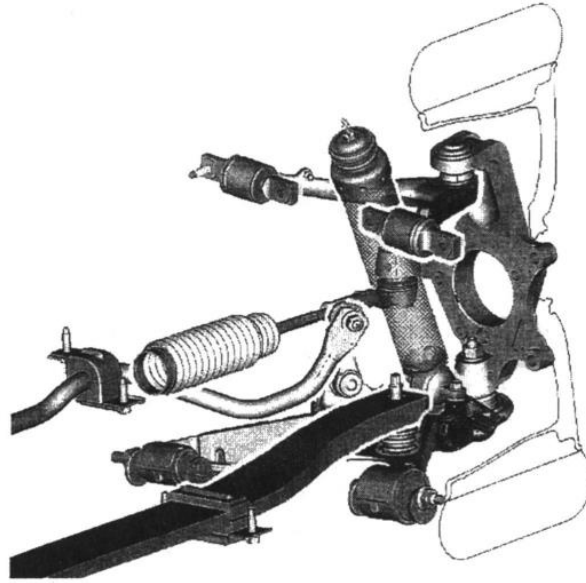


Figure 11 Chevrolet Corvette Suspension System with Leaf Spring

2.1.2.1. Pseudo Rigid Body Method

Pseudo rigid body method (PRBM) is used to determine rigid body equivalent of a compliant mechanism. A compliant mechanism can be synthesized using PRBM on an existing rigid body mechanism.

There are two main types of compliant joints; fixed free compliant beam and small length flexural pivot. These pseudo joints are used to design the desired compliant mechanism using PRBM. Fixed free compliant beam is a link which deflects on its entire body and it is presented in Figure 12 [11].

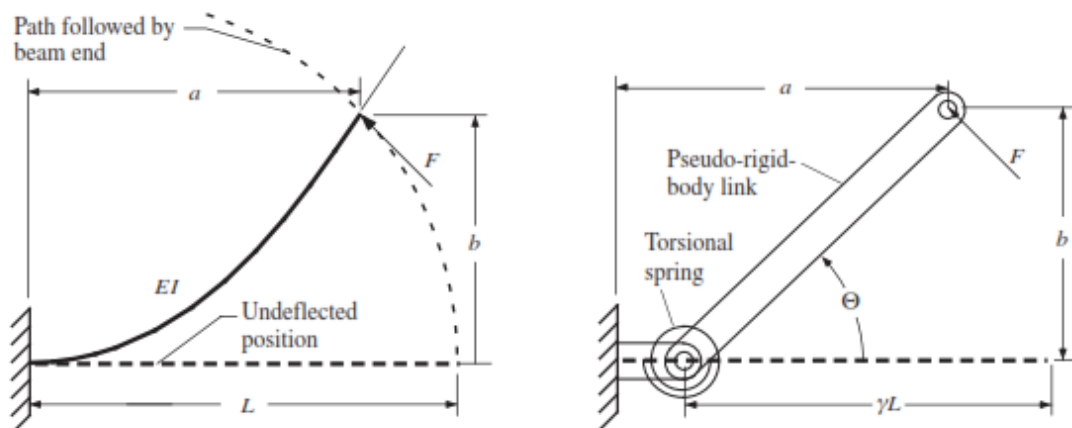


Figure 12 Fixed Free Compliant Beam and Rigid Body Equivalent [11]

Small length flexural pivot is a link which is only compliant on its thin section and thick section is assumed rigid. This pseudo joint is presented in Figure 13.

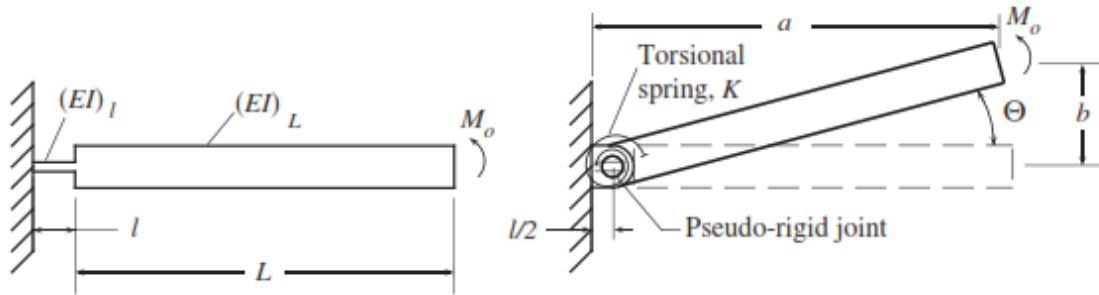


Figure 13 Small Length Flexural Pivot and Rigid Body Equivalent [11]

PRBM can be used to design a four-bar mechanism for a desired geometry. An example compliant four bar mechanism can be seen in Figure 14. This is the main type of compliant mechanism which will be used in this paper to create a compliant equivalent of a rigid link mechanism.

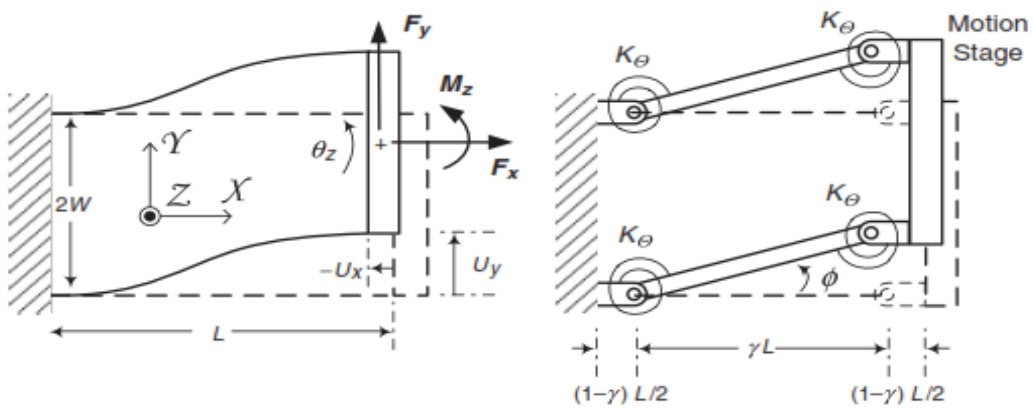


Figure 14 Compliant Four Bar Mechanism and Rigid Body Equivalent [11]

3. METHODOLOGY

A 1/5 remote controlled (RC) scale car is used as a platform to employ compliant suspension design methodology in this thesis. This RC has double wishbone suspension all around. Scale car's rear left suspension is used to assess the compatibility mentioned above. Rear right suspension is kept as it is to have a control sample.

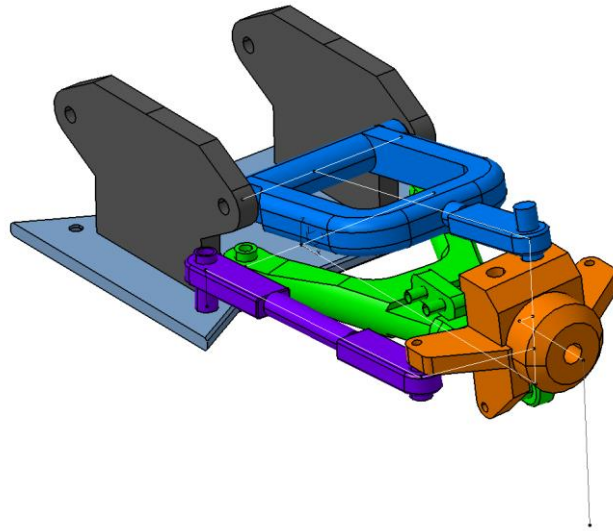


Figure 15 Scale Car Rigid Link Suspension 3D Model

The kinematic parameters of the rigid body suspension and mechanism properties like link lengths and joint positions are obtained from the RC car platform. A picture of the scale car rigid body suspension is presented in Figure 16. The data obtained from the geometry is used to construct a 3D model of the reference rigid body suspension mechanism in Catia (Figure 15). Also, weights of the suspension links of the scale car are measured and presented in Table 2.

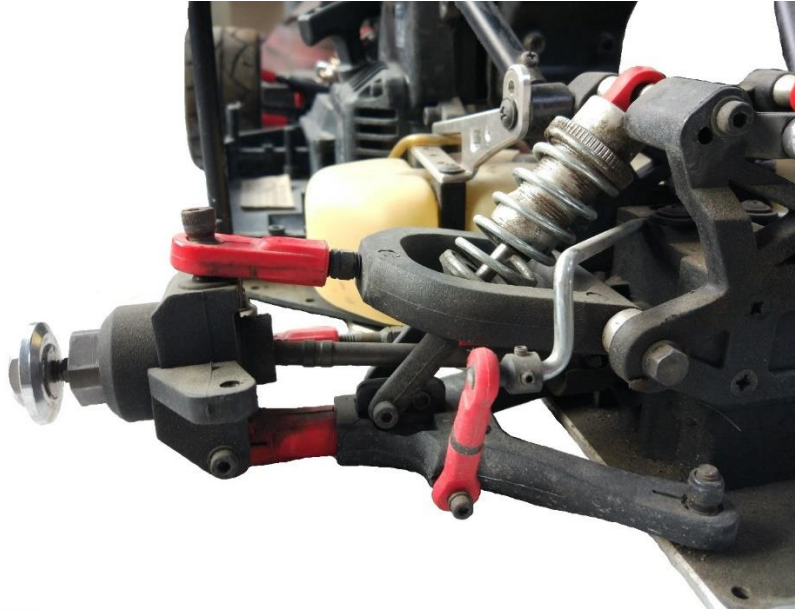


Figure 16 Scale Car Rigid Body Suspension

Table 2 Suspension Components' Weights

Component	Weight (g)
Wheel	248
Tie Rod	34
Knuckle	60
Damper	40
Spring	20
Upper Wishbone	80
Lower Wishbone	76
Half Shaft	112
Suspension Fasteners	41

Total weight of the car is 11 kg. Weight distribution ratio is 55/45 (front/rear). This data is used in suspension calculations.

Spring constant is determined with Eq. (3.1).

$$k = \frac{Gd^4}{8D^3n_a} \quad (3.1)$$

The spring constant “ k ” can be found with spring’s geometrical properties and the spring material's shear modulus “ G ”. Shear modulus is found from the material's elastic modulus

“ E ” and Poisson ratio “ n ”. “ D ” is the mean diameter of the spring, “ d ” is the wire diameter of the spring and “ n_a ” is the number of coils.

After determining required dimensional and mechanical properties, kinematic analysis of the mechanism must be performed to find the properties like camber angle, toe angle etc. These properties then will be used to construct the rigid link equivalent of the original mechanism. Equivalent of the original mechanism must be smaller in size to achieve a similar sized compliant mechanism with respect to the original rigid link mechanism. The reason for that is of the compliant mechanisms requires more space than their rigid body equivalents. This can be easily seen in Figure 14. The compliant links are clearly longer than their rigid equivalents.

Compliant equivalent of the equivalent rigid link mechanism will be synthesized using pseudo rigid body method. During the synthesis procedure, multiple iterations are performed in order to get the acceptable design considering the requirements of the original suspension mechanism.

3.1. Suspension Analysis Method

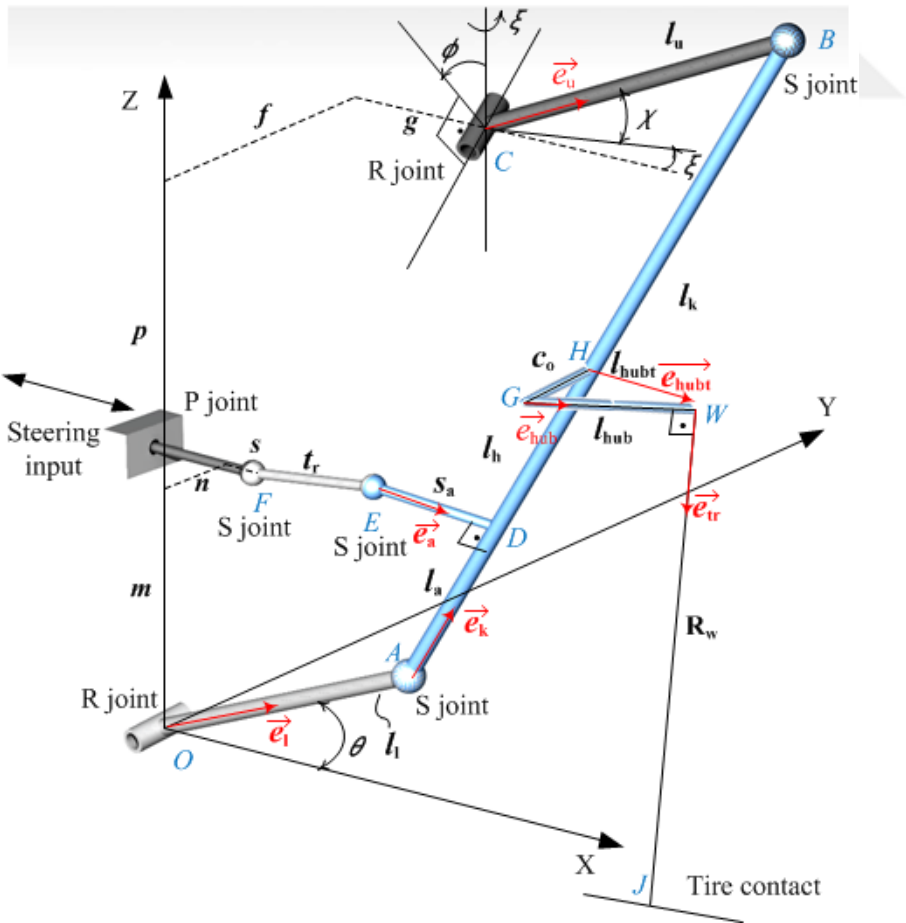


Figure 17 Double Wishbone Suspension Mechanism Parameters [5]

The double wishbone mechanism is essentially formed by RSSR and SSP linkages. In the literature, Tanık and Parlaktaş proposed an analytical approach method to determine kinematic analysis of the double wishbone suspension mechanism [5]. This procedure is employed here as follows:

Definitions of the variables used are presented in Table 3.

Table 3 Suspension Analysis Variables

Variable	Description
ξ	Yaw Angle
ϕ	Anti-Dive Angle
l_l	Length of Lower Wishbone $ OA $
l_u	Length of Upper Wishbone $ BC $
l_k	Length of Knuckle $ AB $
t_r	Length of Tie Rod or Control Arm $ FE $
s_a	Length of Steering Arm $ ED $
l_{hub}	Length of Hub $ GW $
l_a	$ AD $
l_h	$ AH $
c_0	Caster Offset $ HG $
l_{hubt}	$ HW $
\vec{e}_i	Unit Vector on i^{th} Link
R_w	Effective Tire Radius $ WJ $
θ	Lower Wishbone Angle
χ	Angular Displacement of Upper Wishbone

Kinematic analysis of the rear suspension mechanism of the scale car is made with two independent loops which are OABCO and OADEF0 (Figure 3). Loop of the RSSR linkage is analyzed first and ball joint F is considered to be fixed at a specific point. Analysis [5] can be performed with a given set of lower wishbone angles while l_l , l_u , l_k , ξ and ϕ is known.

$$|\overline{AB}| = |\overline{OB} - \overline{OA}| \quad (3.2)$$

Where:

$$|\overline{OA}| = l_l \sin \theta \vec{i} + l_l \sin \theta \vec{k} \quad (3.3)$$

$$\begin{aligned} |\overline{OA}| = & (g + l_u \cos \chi \cos \xi + l_u \sin \chi \sin \phi \sin \xi) \vec{i} \\ & + (f + l_u \cos \chi \cos \xi - l_u \sin \chi \sin \phi \cos \xi) \vec{j} \\ & + (p + l_u \sin \chi \cos \phi) \vec{k} \end{aligned} \quad (3.4)$$

General displacement equation of the RSSR linkage is as follows:

$$\begin{aligned} k_1 + (k_2 - k_3 \cos \theta) \cos \chi - (k_4 + k_5 \sin \theta - k_6 \cos \theta) \sin \chi \\ - k_7 \cos \theta - k_8 \sin \theta = 0 \end{aligned} \quad (3.5)$$

Where:

$$k_1 = f^2 + g^2 + p^2 + l_l^2 + l_u^2 - l_k^2 \quad (3.6)$$

$$k_2 = 2fl_u \sin \xi + 2gl_u \cos \xi \quad (3.7)$$

$$k_3 = 2l_l l_u \cos \xi \quad (3.8)$$

$$k_4 = 2fl_u \cos \xi \sin \phi - 2pl_u \cos \phi - 2gl_u \sin \xi \sin \phi \quad (3.9)$$

$$k_5 = 2l_l l_u \cos \phi \quad (3.10)$$

$$k_6 = 2l_l l_u \sin \xi \sin \phi \quad (3.11)$$

$$k_7 = 2gl_l \quad (3.12)$$

$$k_8 = 2pl_l \quad (3.13)$$

Values of χ can be found for a given set of θ angles from Eq. (3.5) by applying half tangent formula and substituting values of k_i :

$$\chi = 2 \tan^{-1} \left(\frac{-B \pm \sqrt{B^2 - 4AC}}{2A} \right) \quad (3.14)$$

Where:

$$A = -k_1 + k_2 - k_3 \cos \theta + k_7 \cos \theta + k_8 \sin \theta \quad (3.15)$$

$$B = 2k_4 + 2k_5 \sin \theta + 2k_6 \cos \theta \quad (3.16)$$

$$C = -k_1 - k_2 - k_3 \cos \theta + k_7 \cos \theta + k_8 \sin \theta \quad (3.17)$$

$$\overline{AB} = l_k \overline{e_k} \quad (3.18)$$

The position vector of the knuckle is given by Eq. (3.18) and the unit vector " $\overline{e_k}$ " of the knuckle can be determined with Eq. (3.19).

$$\overline{e_k} = \frac{1}{l_k} \begin{bmatrix} g + l_u \cos \chi \cos \xi + l_u \sin \chi \sin \phi \sin \xi - l_l \cos \theta \\ f + l_u \cos \chi \cos \xi - l_u \sin \chi \sin \phi \sin \xi \\ p + l_u \sin \chi \cos \phi - l_l \sin \theta \end{bmatrix} \quad (3.19)$$

Unit vector of lower wishbone is given by Eq. (3.20).

$$\vec{e}_l = [\cos \theta \quad 0 \quad \sin \theta]^T \quad (3.20)$$

Positions of the knuckle and the wishbones can be determined using Eqns. (3.21), (3.22) and (3.27) for a given set of θ in closed equation set.

For the loop of the SSP linkage, OADEF loop is analyzed. Toe variation due to suspension travel can be obtained with this analysis.

Because the tie rod length: $t_r = |\vec{EF}|$ and the control arm length: $s_a = |\vec{EA} \times \vec{EB}|/|\vec{BA}|$ are constant it can be stated that:

$$t_r^2 = (E_x - F_{x0})^2 + (E_y - F_{y0})^2 + (E_z - F_{z0})^2 \quad (3.21)$$

$$s_a^2 = (D_x - D_{x0})^2 + (D_y - D_{y0})^2 + (D_z - D_{z0})^2 \quad (3.22)$$

Where:

$$\vec{D} = l_l \vec{e}_l + l_a \vec{e}_k \quad (3.23)$$

$$l_a = \sqrt{|\vec{AE}|^2 - s_a^2} \quad (3.24)$$

Steering arm vector and knuckle vector are perpendicular to each other ($\vec{ED} \perp \vec{AD}$) for every position of the mechanism. Because the scalar product of perpendicular vectors is zero:

$$\vec{ED} \cdot \vec{AD} = 0 \quad (3.25)$$

$$(l_l \vec{e}_l + l_a \vec{e}_k - (E_x \vec{i} + E_y \vec{j} + E_z \vec{k})) \cdot (l_a \vec{e}_k) = 0 \quad (3.26)$$

Rearranging the Eq. (3.26):

$$c_1 E_x + c_2 E_y + c_3 E_z + c_4 = 0 \quad (3.27)$$

Known parameters for the Eq. (3.27) are:

$$c_1 = -l_a \vec{e}_{k_x} \quad (3.28)$$

$$c_2 = -l_a \vec{e}_{k_y} \quad (3.29)$$

$$c_3 = -l_a \vec{e}_{k_z} \quad (3.30)$$

$$c_4 = l_a^2 + l_l l_a (\vec{e}_{k_x} \vec{e}_{l_x} + \vec{e}_{k_y} \vec{e}_{l_y} + \vec{e}_{k_z} \vec{e}_{l_z}) \quad (3.31)$$

New coordinates of the spherical joint E of the steering arm are E_x , E_y and E_z . These parameters are the unknowns of Eqns. (3.21), (3.22) and (3.27). Because three unknowns can be solved with three equations, all positions of the joints are determined.

In suspension analyses variations of camber, caster, kingpin, toe angle and track are given in terms of wheel travel. This analysis specifies lower wishbone angle as an input and corresponding wheel travel is calculated.

$$\vec{e}_{hub_n} = [\cos \varepsilon_0 \quad 0 \quad \sin \varepsilon_0]^T \quad (3.32)$$

ε_0 is the positive static camber position of wheel (Figure 3).

$$\vec{l}_{hubt_0} = c_0[0 \quad -1 \quad 0]^T + l_{hub}\vec{e}_{hub_0} \quad (3.33)$$

\vec{l}_{hubt_0} is the static position of the wheel center.

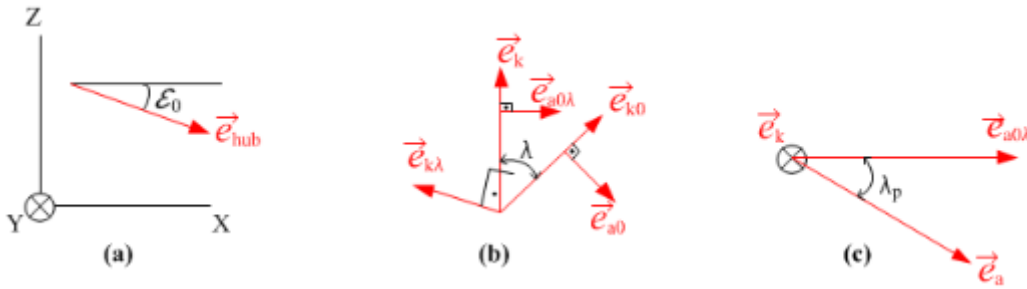


Figure 18 Vector Transformations

Rotation matrices are used to obtain the position vectors on the knuckle. Because caster offset, hub and steering arm are on the same rigid body, they will all have the same rotation during motion of the suspension. This means if rotation of any unit vector is found, other unit vectors can be found using associated rotation matrices.

Rotation of knuckle is considered to be superposition of two different rotations in this part and rotation around its own axis is disregarded. Unit vector \vec{e}_k is calculated from Eqn. (3.19) for every θ , rotation of \vec{e}_k can be found as following:

$$\lambda = \sin^{-1}[(\vec{e}_{k_0} \times \vec{e}_k) \cdot \vec{e}_{k_\lambda}] \quad (3.34)$$

$$\vec{e}_{k_\lambda} = (\vec{e}_{k_0} \times \vec{e}_k) / |\vec{e}_{k_0} \times \vec{e}_k| \quad (3.35)$$

$$\lambda_p = \sin^{-1}[(\vec{e}_{a_0\lambda} \times \vec{e}_a) \cdot \vec{e}_{k_\lambda}] \quad (3.36)$$

Rotation matrix:

$$R(\vec{u}, \theta) = \begin{bmatrix} \cos \theta + u_x^2 H & u_x u_y H - u_z \sin \theta & u_x u_z H - u_y \sin \theta \\ u_y u_x H - u_z \sin \theta & \cos \theta + u_y^2 H & u_y u_z H - u_x \sin \theta \\ u_z u_x H - u_y \sin \theta & u_z u_y H - u_x \sin \theta & \cos \theta + u_z^2 H \end{bmatrix} \quad (3.37)$$

Where:

$$H = 1 - \cos \theta \quad (3.38)$$

Since the associated rotation matrices are found, the unit vector \vec{e}_{hub} can be calculated using Eqn. (3.39).

$$\vec{e}_{hub} = R(\vec{e}_k, \lambda_p) R(\vec{e}_{k\lambda}, \lambda) \vec{e}_{hub_n} \quad (3.39)$$

Any position of the wheel hub \vec{e}_{hubt} can be determined using the same rotation matrices using Eqns. (3.40) and (3.40).

$$\vec{e}_{hubt} = R(\vec{e}_k, \lambda_p) R(\vec{e}_{k\lambda}, \lambda) \vec{e}_{hubt_0} \quad (3.40)$$

$$\vec{l}_{hubt} = \vec{e}_{hubt} l_{hubt} \quad (3.41)$$

Vector between the points WJ needs to be determined. The unit vector of this vector \vec{e}_{tr} must be on XZ plane: $\vec{e}_{tr} = [t_{rx} \quad 0 \quad t_{rz}]^T, t_{rx}^2 + t_{rz}^2 = 1$

\vec{e}_{tr} is perpendicular to \vec{e}_{hub} because it is the wheel rotation axis. Because of this, $\vec{e}_{hubx} \cdot t_{rx} + \vec{e}_{hubz} \cdot t_{rz} = 0$

$$\vec{e}_{tr} = \begin{bmatrix} \pm \frac{\vec{e}_{hubz}}{\vec{e}_{hubx}} \sqrt{\frac{1}{\left(\frac{\vec{e}_{hubz}}{\vec{e}_{hubx}}\right)^2 + 1}} & 0 & \pm \sqrt{\frac{1}{\left(\frac{\vec{e}_{hubz}}{\vec{e}_{hubx}}\right)^2 + 1}} \end{bmatrix}^T \quad (3.42)$$

$$\Delta \vec{OJ} = \vec{OJ} - \vec{OJ}_0 \quad (3.43)$$

Wheel travel is given by Eqn. (3.43). It can be determined by using Eqns. (3.19), (3.20), (3.40) and (3.42).

$$\Delta \vec{OJ} = (l_l \vec{e}_l + l_h \vec{e}_k + l_{hubt} + R_w \vec{e}_{tr}) - (l_l \vec{e}_{l_0} + l_h \vec{e}_{k_0} + l_{hubt_0} + R_w \vec{e}_{tr_0}) \quad (3.44)$$

$\Delta \vec{OJ}_z$ is the suspension wheel travel and $2\Delta \vec{OJ}_x$ is the track variation.

Camber, caster, kingpin and toe angles are measured as shown in Figure 19.

$$\varphi = \cos^{-1}(\overrightarrow{e_{hub}} \cdot \vec{k}) - \pi/2 \quad (3.45)$$

$$\tau = \cos^{-1}(\overrightarrow{e_k} \cdot \overrightarrow{e_{caster}}) - \pi/2 \quad (3.46)$$

$$\overrightarrow{e_{caster}} = \left[\pm \frac{e_{huby}}{e_{hubx}} \sqrt{\frac{1}{\left(\frac{e_{huby}}{e_{hubx}}\right)^2 + 1}} \quad \pm \sqrt{\frac{1}{\left(\frac{e_{huby}}{e_{hubx}}\right)^2 + 1}} \quad 0 \right]^T \quad (3.47)$$

$$\sigma = \cos^{-1}(\overrightarrow{e_k} \cdot \overrightarrow{e_{hubp}}) - \pi/2 \quad (3.48)$$

$$\overrightarrow{e_{hubp}} = [e_{hubpx} \quad e_{hubpy} \quad 0]^T / \sqrt{e_{hubpx}^2 + e_{hubpy}^2} \quad (3.49)$$

$$\beta = \pi/2 - \cos^{-1}(\overrightarrow{e_{hubp}} \cdot \vec{j}) \quad (3.50)$$

Positive values of β are toe-in and negative values are toe-out.

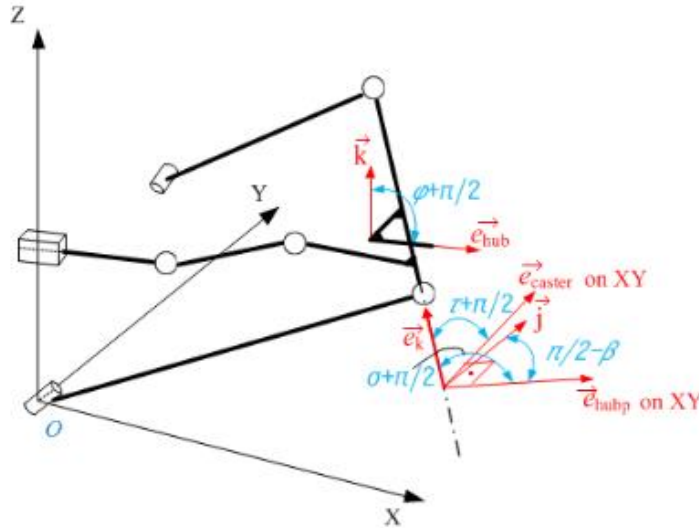


Figure 19 Camber, Caster, Kingpin and Toe Angle Measurement [5]

3.2. Rigid Body Suspension Analysis

The parameters of the rear suspension of the scale car are measured from the constructed 3D model in Catia. The values presented in Table 4 are the required numerical values of the analysis method given in Section 3.1.

Table 4 Suspension Analysis Parameters

Variable	Value	Unit
l_l	130	mm
l_u	122.4	mm
l_k	56.7	mm
p	33	mm
g	10	mm
f	1	mm
l_h	26.4	mm
c_0	-5.6	mm
l_{hub}	36.8	mm
E_0	$[120.1 \ 41.2 \ 13.3]^T$	mm
ϕ	0	degrees
ξ	0	degrees
ε_0	-1	degrees
R_w	62	mm

The wheel travel is 37.4 mm. These variables are measured to be used in the suspension analysis regarding most important kinematic variables for a suspension system [15] such as camber, caster, toe variation, etc... using the analytical double wishbone solution algorithm in suspension analysis method section. Suspension analysis is made on MATHCAD software. The camber, caster, kingpin, half-track and toe variation plots of the rigid link mechanism are presented in Figure 20 though Figure 24.

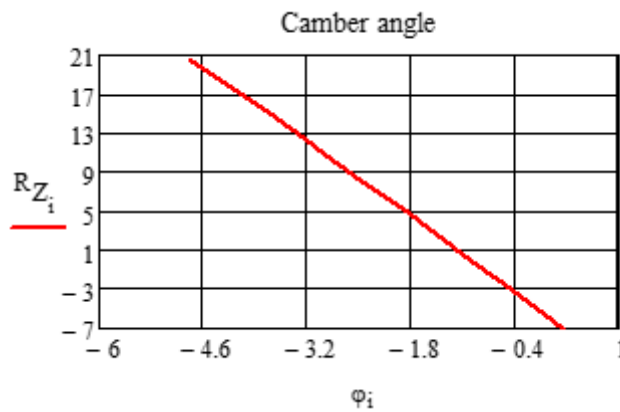


Figure 20 Rigid Link Mechanism Camber Variation

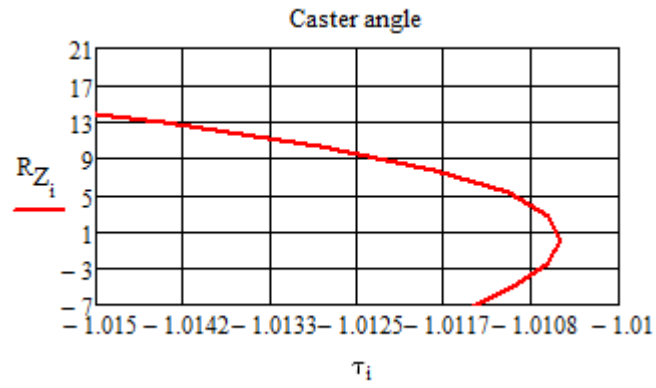


Figure 21 Rigid Link Mechanism Caster Variation

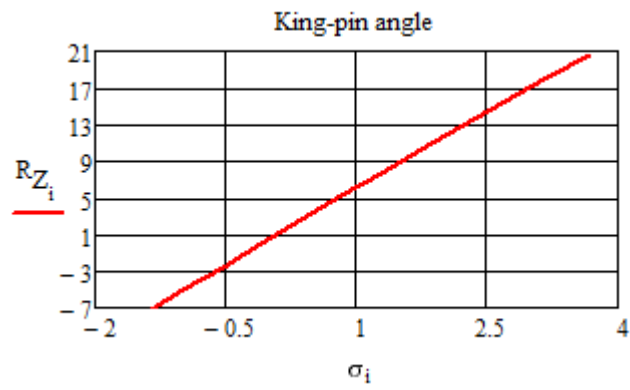


Figure 22 Rigid Link Mechanism Kingpin Variation

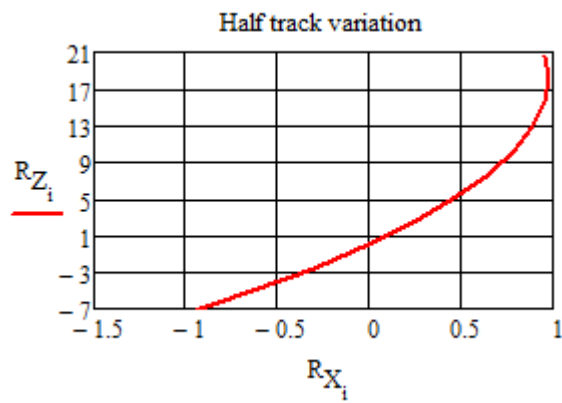


Figure 23 Rigid Link Mechanism Half Track Variation

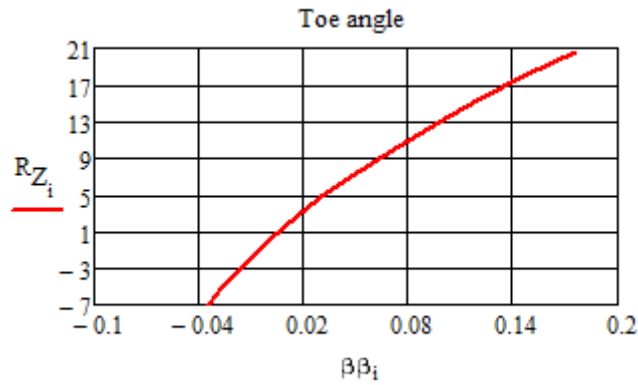


Figure 24 Rigid Link Mechanism Toe Variation

The above Figures show us the kinematic characteristics of the RC car's rear suspension. In the next sections, a compliant suspension mechanism that possesses similar kinematic characteristics as the rigid one will be designed.

3.3. Construction of Rigid Body Equivalent of the Desired Compliant Mechanism

Compliant equivalent of the rigid link suspension mechanism needs to be constructed from a smaller mechanism to insert the RC car's chassis. A comparison of the compliant mechanism and its rigid body equivalent is presented in Figure 25. The white wireframe is the rigid mechanism link and blue one is the compliant mechanism. As it is apparent, rigid body equivalent of a compliant mechanism is significantly smaller.

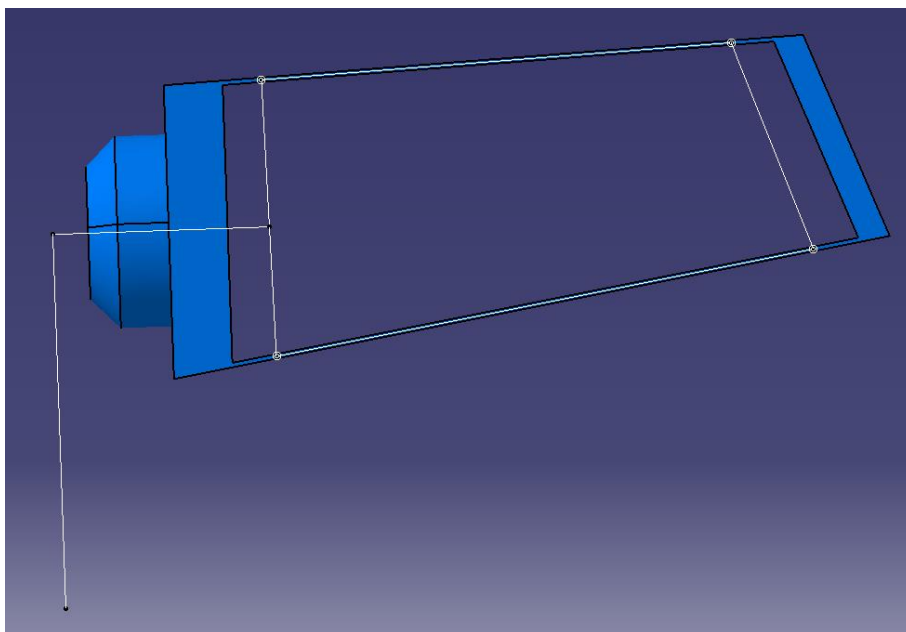


Figure 25 Rigid Body Equivalent and Desired Compliant Mechanism

PRBM of a compliant mechanism is smaller than the compliant version. If the compliant mechanism was constructed using the rigid link suspension mechanism of the scale car, compliant equivalent would be bigger than the rigid mechanism and implementation to an existing car wouldn't be possible.

An Approach used in this phase to obtain a compliant mechanism with appropriate size is to use a ratio which is determined intuitively to scale down all suspension links. After analyzing this scaled mechanism, it is observed that another approximation is needed to make the mechanism follow the desired path.

The variables are chosen by trial and error method while checking the results of the analysis on every step to obtain a mechanism having similar suspension kinematics characteristics with the original one.

The parameters of the rigid link equivalent (PRBM) of the compliant suspension mechanism are presented in Table 5. These values are used to construct the compliant equivalent of this rigid mechanism.

Table 5 Parameters of the Rigid Link Equivalent of Compliant Mechanism

Variable	Value	Unit
l_l	93	mm
l_u	80	mm
l_k	47	mm
p	35	mm
g	14	mm
f	0	mm
l_h	22	mm
c_0	0	mm
l_{hub}	36.8	mm
ϕ	0	degrees
ξ	0	degrees
ε_0	-1	degrees
R_w	62	mm

Camber, caster, kingpin, half-track and toe variation plots of the equivalent rigid link mechanism are presented in Figure 26 through Figure 30.

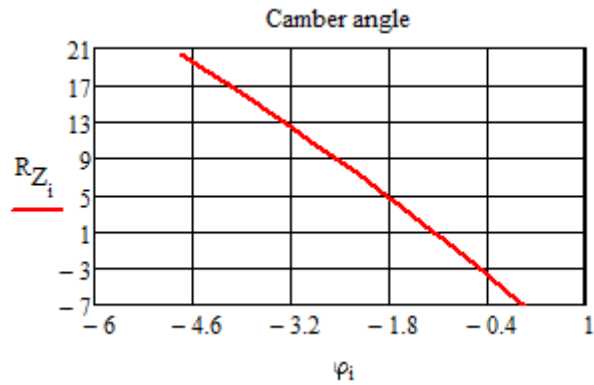


Figure 26 Equivalent Rigid Link Mechanism Camber Variation

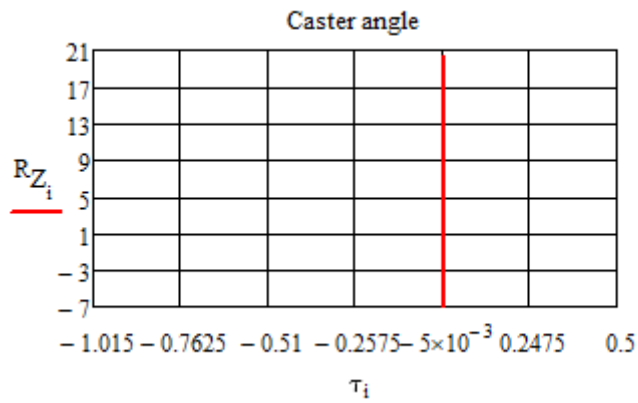


Figure 27 Equivalent Rigid Link Mechanism Caster Variation

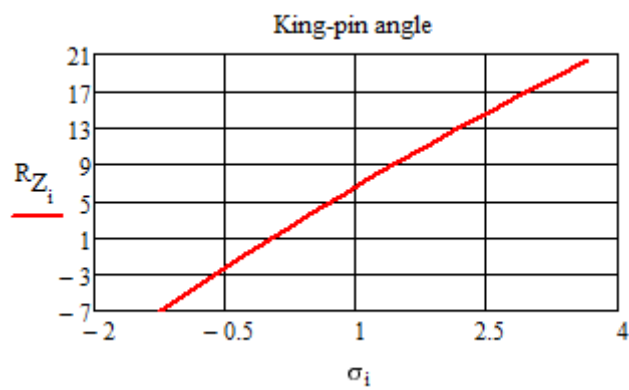


Figure 28 Equivalent Rigid Link Mechanism Kingpin Variation

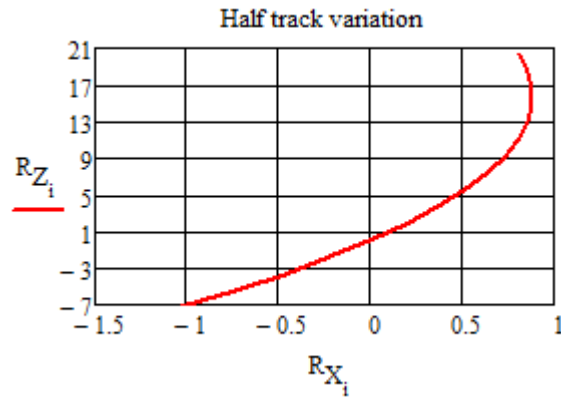


Figure 29 Equivalent Rigid Link Mechanism Half Track Variation

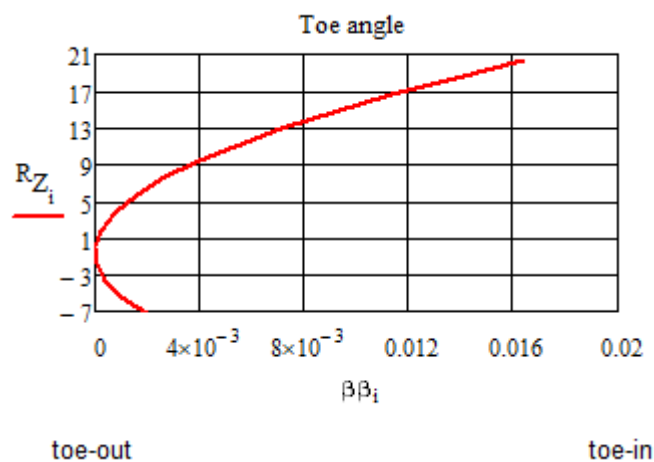


Figure 30 Equivalent Rigid Link Mechanism Toe Variation

The main design criteria of the equivalent rigid link mechanism is getting as close as possible to the original mechanism concerning kinematic characteristics presented in above figures. The camber and king-pin angle variations are virtually the same between two mechanisms. The caster and toe angle variations are both negligible. Only visible difference in two mechanisms is in half-track variation and it is by a small margin. Equivalent mechanism has 10% more variation in half track.

3.4. Equivalent Spring Rate Calculation of the Compliant Suspension

In this section, equivalent spring rate of the constructed rigid body equivalent mechanism is designed. Virtual work method is used to determine the required rotational spring stiffness of the compliant segments.

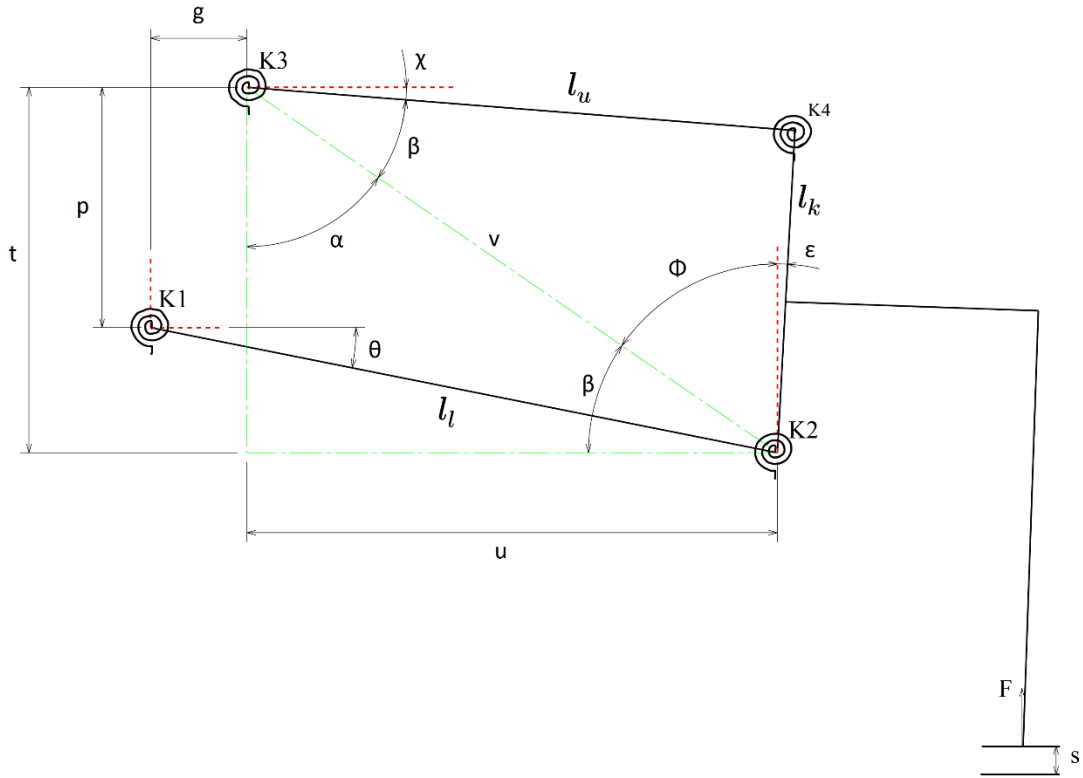


Figure 31 Simplified Expression for the 2D Mechanism Undeformed Position

Undeformed position of the compliant mechanism is the rebound position of the rigid link mechanism. This way, stiffness of the compliant segments is used instead of a coil spring. Required torsional spring stiffnesses are calculated by using Eqns. (3.51) and (3.52).

$$K_1 := 2 \cdot \gamma \cdot K_\theta \cdot \frac{E \cdot I}{l_{lc}} \quad (3.51)$$

$$K_3 := 2 \cdot \gamma \cdot K_\theta \cdot \frac{E \cdot I}{l_{uc}} \quad (3.52)$$

At this stage, the mechanism we need to apply the virtual work method is planar and we can use the following geometrical expressions to simplify the calculations.

Lengths of the sides of the imaginary green right triangle is calculated as in Eqns. (3.53), (3.54) and (3.55).

$$v := \sqrt{t^2 + u^2} \quad (3.53)$$

$$t := p - l_l \cdot \sin(\theta) \quad (3.54)$$

$$u := l_l \cdot \cos(\theta) - g \quad (3.55)$$

Angles of the triangle is calculated with Eqns. (3.56) and (3.57).

$$\alpha := \text{atan}\left(\frac{u}{t}\right) \quad (3.56)$$

$$\beta := \frac{\pi}{2} - \alpha \quad (3.57)$$

Angles formed between hypotenuse of the green triangle and upper wishbone, lower wishbone is calculated with Eqns.(3.58) and (3.59).

$$\Phi := \text{acos}\left(\frac{v^2 + l_k^2 - l_u^2}{2 \cdot v \cdot l_k}\right) \quad (3.58)$$

$$\Psi := \text{acos}\left(\frac{l_u^2 + v^2 - l_k^2}{2 \cdot v \cdot l_u}\right) \quad (3.59)$$

Knuckle and upper wishbone angles are determined by Eqns. (3.60) and (3.61).

$$\chi := \Psi - \beta \quad (3.60)$$

$$\varepsilon := \frac{\pi}{2} - \beta - \Phi \quad (3.61)$$

Expressions for the work done by the compliant joints can be calculated as in Eqn. (3.62).

These are presented in Figure 31.

$$\delta W_2 = \delta W_{21} + \delta W_{22} + \delta W_{23} + \delta W_{24} \quad (3.62)$$

Where:

$$\delta W_{21} = -K1 \cdot (\theta - \theta_0) \cdot \delta\theta \quad (3.63)$$

$$\delta W_{22} = -K2 \cdot (\theta - \varepsilon - \theta_0 + \varepsilon_0) \cdot (\delta\theta - \delta\varepsilon) \quad (3.64)$$

$$\delta W_{23} = -K3 \cdot (\chi - \varepsilon - \chi_0 + \varepsilon_0) \cdot (\delta\chi - \delta\varepsilon) \quad (3.65)$$

$$\delta W_{24} = -K4 \cdot (\chi - \chi_0) \cdot \delta\chi \quad (3.66)$$

Where:

$$\delta\chi = \frac{l_1 \cdot \cos(\theta) + l_1 \cdot \sin(\theta) \cdot \tan(\varepsilon)}{l_u \cdot \cos(\chi) \cdot (1 + \tan(\chi) \cdot \tan(\varepsilon))} \cdot \delta\theta \quad (3.67)$$

$$\delta\varepsilon = \frac{l_1 \cdot \cos(\theta) \cdot \tan(\chi) - l_1 \cdot \sin(\theta)}{l_k \cdot \cos(\varepsilon) \cdot (1 + \tan(\chi) \cdot \tan(\varepsilon))} \cdot \delta\theta \quad (3.68)$$

Work done by the quarter car sprung weight force can be expressed as in Eqns. (3.69) and (3.70).

$$\delta W_1 = F \cdot \delta s \quad (3.69)$$

$$\delta s = l_l \cdot \cos(\theta) \cdot \delta\theta - l_a \cdot \sin(\varepsilon) \cdot \delta\varepsilon \quad (3.70)$$

General expression for the virtual work method is presented in Eqn. (3.71).

$$\delta W_1 + \delta W_2 = 0 \quad (3.71)$$

Substituting Eqns. (3.62) and (3.69) into Eqn. (3.71) yields the general virtual work method expression.

Rearranging the Eqn. (3.71) we can get the force expression,

$$F_a = \frac{K1 \cdot (\theta - \theta_0) \cdot \delta\theta + K1 \cdot (\theta - \varepsilon - \theta_0 + \varepsilon_0) \cdot (\delta\theta - \delta\varepsilon)}{\delta s} \quad (3.72)$$

$$F_b = \frac{K3 \cdot (\chi - \varepsilon - \chi_0 + \varepsilon_0) \cdot (\delta\chi - \delta\varepsilon) + K3 \cdot (\chi - \chi_0) \cdot \delta\chi}{\delta s} \quad (3.73)$$

$$F = F_a + F_b \quad (3.74)$$

The equivalent spring constant is the effective spring constant at the tire ground contact. Assuming the kingpin angle is approximately perpendicular to the lower wishbone, The equivalent spring constant can be determined from Eqn. (3.75) [16]. Unknowns from the Eqn. is presented in Figure 32.

$$k_{eq} := k \cdot \left(\frac{a}{b} \cdot \cos(\iota) \right)^2 \quad (3.75)$$

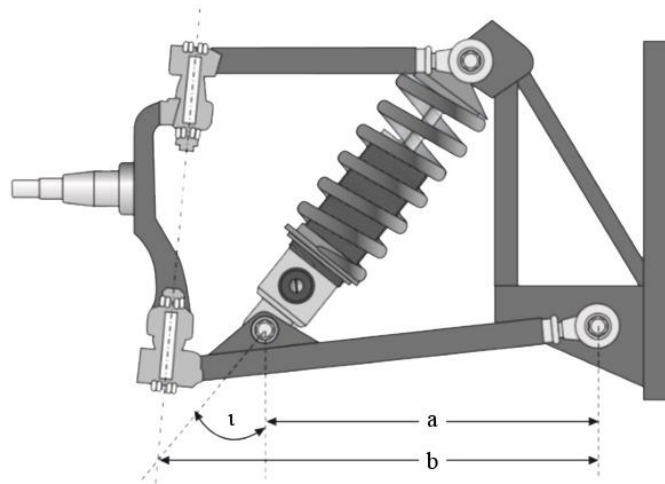


Figure 32 Equivalent Spring Constant Parameters

After this stage, using the suspension geometry determined in part 3.3 and changing the free parameters, desired reaction force of the compliant suspension system can be found.

3.5. A Novel Approach to Increase Stiffness of the Compliant Suspension Mechanism

While calculating the stiffness, thickness and width of the compliant segment is used as free parameters and both wishbones are the same with respect to thickness and width.

Maximum stress that will occur at any fixed guided compliant mechanism section can be calculated with following formula [7],

$$\sigma_{max} := \frac{P \cdot a_u \cdot c_u}{2 \cdot I_2} \quad (3.76)$$

Single – single layer formation is using a single layer of compliant material in the direction of thickness and it is presented in Figure 25. This formation is used for upper and lower compliant sections at first, but it resulted in very high levels of bending stress.

In order to reduce the stresses at these critical regions, we proposed an original approach in this study: Possibility of using double layer in either or both compliant sections. As it can be observed from Figure 33, a compliant suspension with lower double layer compliant section is presented. This original design increases stiffness of the suspension without increasing the compliant segment's thickness. The increase in the thickness of a beam causes a stress increase for the same deflection. With this approach this disadvantage is eliminated. It should also be noted that this design is not similar to the multi-leaf spring design. A multi-leaf spring is made up of a single leaf with additional leaves attached to it using spring clamps. The additional leaves make the spring stiffer, allowing it to carry greater loads. As a multi-leaf spring operates, friction is generated between the leaves, causing it to have a dampening characteristic. However, in our design there is no contact between the layers that causes both friction and shear stress on the surface of the compliant segment.

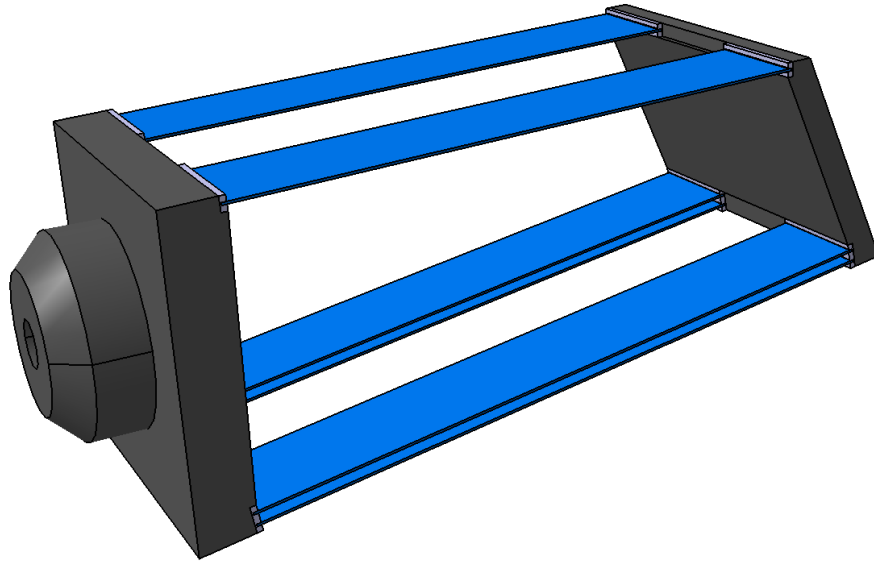


Figure 33 3D Model of the Compliant Mechanism

3.6. Design of the Compliant Mechanism by using Rigid Body Replacement Technique

Compliant mechanism is synthesized using the parameters from the equivalent rigid link mechanism. While this synthesis, cross sectional dimensions are determined using virtual work method. While synthesizing, Single – single layer formation presented in Figure 25 resulted in high levels of stress and design approach is changed to single – double layer formation presented in Figure 33.

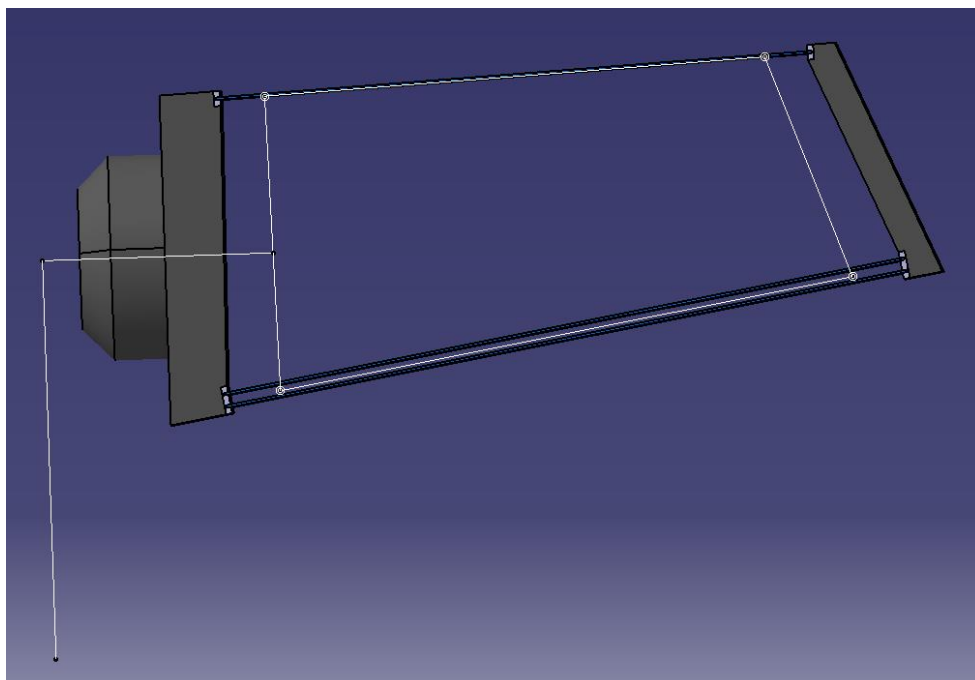


Figure 34 Single-Double Layer Compliant Mechanism and Rigid Link Equivalent

Layers of the compliant wishbone sections are positioned as two separate sections with spacing between them (Figure 33). This design approach is used to increase the torsional rigidity of the system. Disadvantages of using fixed guided compliant segments for wishbones include high stresses which occur during braking [17] but the design approach mentioned before reduces those stresses as well.

After determining the parameters using the equivalent rigid link mechanism parameters by PRBM, final form of the compliant mechanism is constructed.

Compliant mechanism parameters are presented in Table 6.

Table 6 Compliant Mechanism Parameters

Variable	Value	Unit
l_{lc}	109	mm
l_{uc}	94	mm
b_u	35	mm
b_l	70	mm
h	0.4	mm

3D model of the synthesized compliant mechanism is created according to the parameters presented in Table 6. Upper and lower connections are made in two-piece configuration to give the system torsional rigidity. Also, two-layer configuration of the lower wishbone adds torsional rigidity to the system as well. Model of the compliant mechanism is presented in Figure 33.

3.7. Verification of the Compliant Mechanism via Finite Element Analysis

Finite element analyses are performed with Ansys. Because deflections caused by the load cases are large deflections, analyses cannot be made using small deflection assumptions.

Interfaces between compliant and rigid sections are designed in a way to eliminate stress concentrations. Cross section of holder geometry of compliant sections is presented in Figure 35. This holder has small radii on the side which compliant section deflects. With the help of this geometry, none or negligible stress concentrations occur at the contact points.

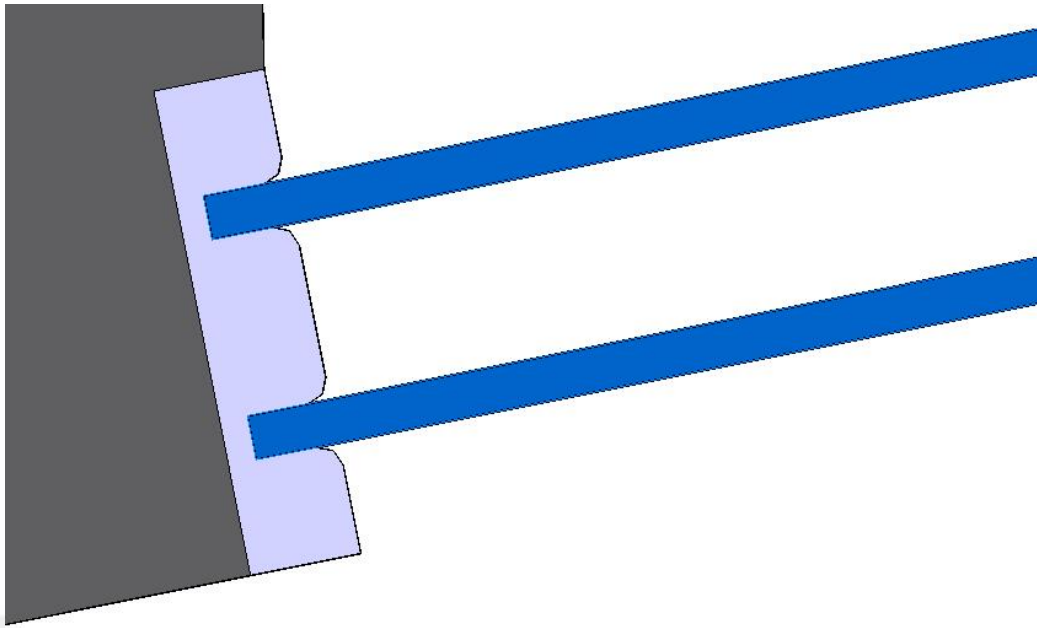


Figure 35 Holder Geometry

Material selected for the compliant sections of the mechanism is blue polished steel. Properties of this material is presented in Table 7.

Table 7 Material Properties of Blue Polished Steel

Density	7800	kg/m^3
Young's Modulus	210	GPa
Poisson's Ratio	0,29	-
Bulk Modulus	166	GPa
Shear Modulus	81	GPa
Yield Strength	1000	MPa
Ultimate Strength	1300	MPa

Meshing of the compliant section of the mechanism is made using hexahedron meshes. This type of mesh is used because it offers high accuracy and hexahedron meshes can fill the geometry perfectly because compliant sections are rectangular prisms. Cross sectional area of the upper wishbone is $1,4 \times 10^{-5} m^2$, its volume is $1,34 \times 10^{-6} m^3$ and there are 1872 nodes. Cross sectional area of the lower wishbone is $2,8 \times 10^{-5} m^2$, its volume is $3,10 \times 10^{-6} m^3$ and there are 3968 nodes Meshing of the model is presented in Figure 36.

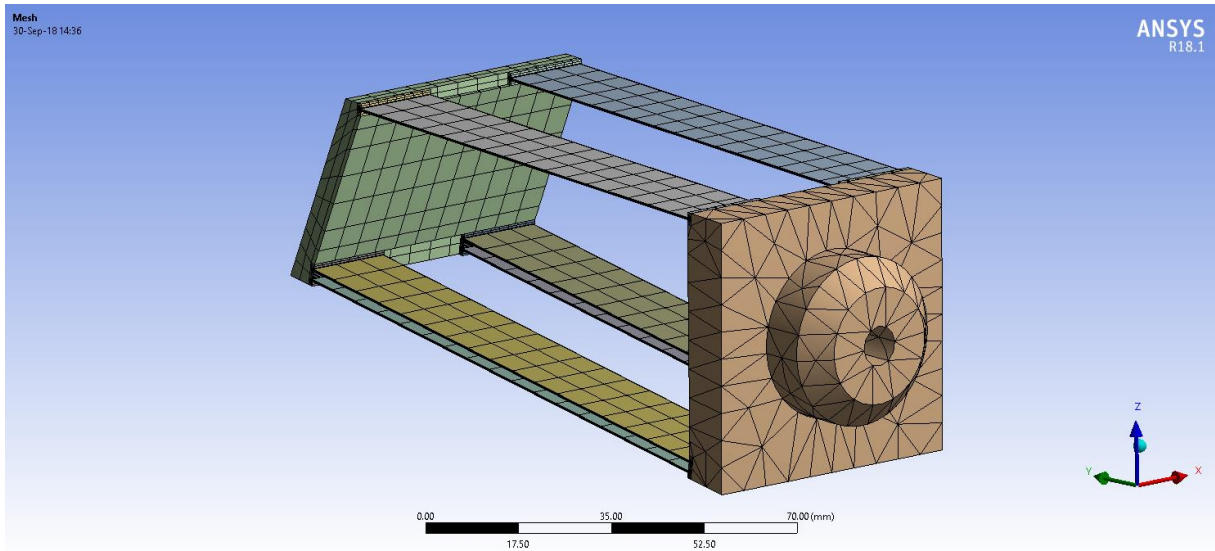


Figure 36 Analysis Model Meshing

Compliant section of the mechanism has 3 meshes along its thickness as it is presented in Figure 37. Using at least three meshes along the geometries thickness ensures low error values.

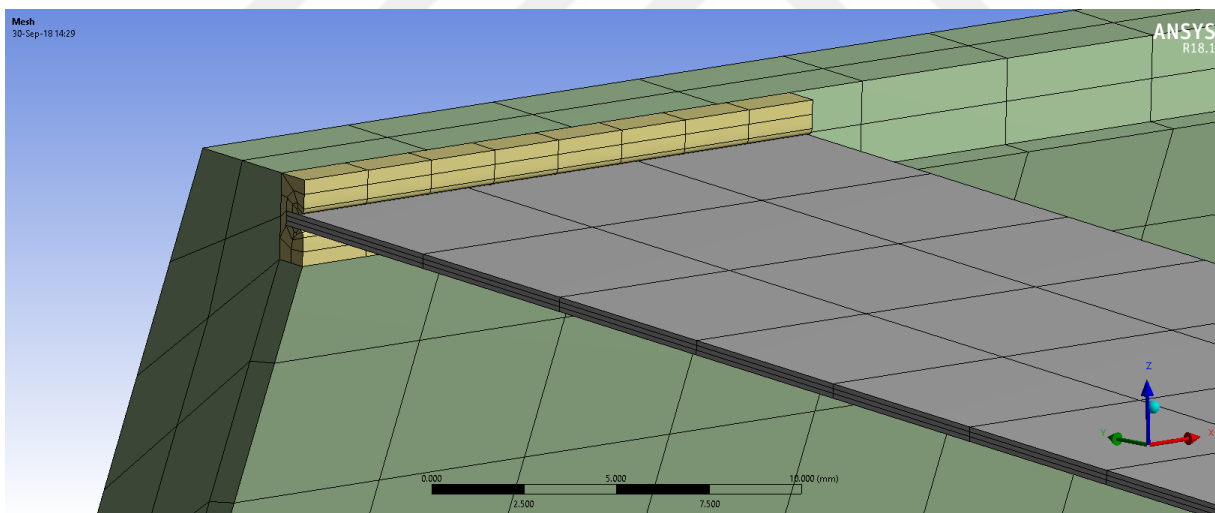


Figure 37 Compliant Section Meshes

To measure rotation of an element in Ansys, a remote point was associated with the element. Remote point needs to be set deformable, therefore it doesn't affect the FEA results. Next, a commands element is inserted under the remote point created earlier. This commands element is used to identify and store the element's movements. Another commands element is inserted under solution to get the necessary angle and rotation values stored in the previous commands element. This latter commands element and the necessary project tree are used

to measure differential angles around x , y and z axes. These angles are presented in Figure 38.

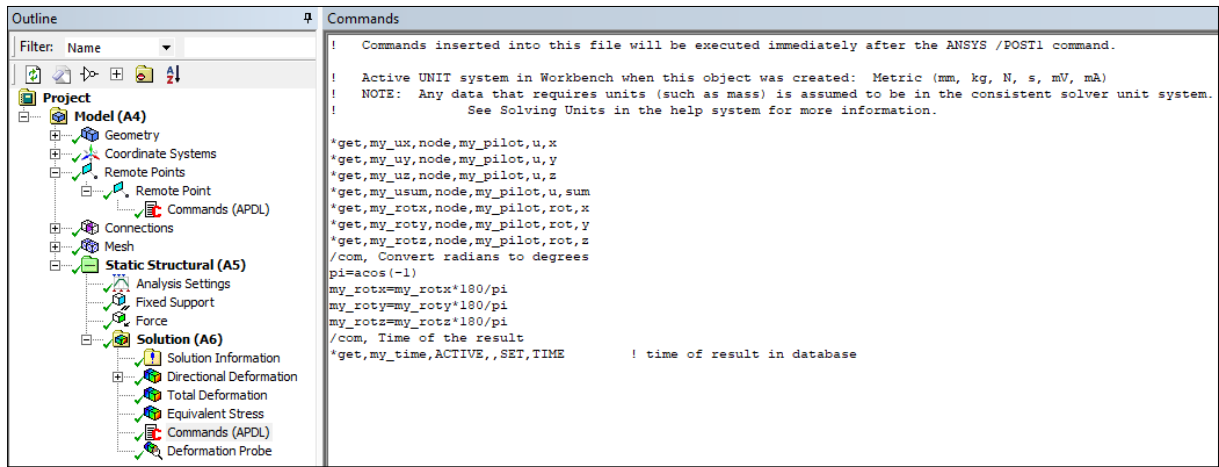


Figure 38 Analysis Project Tree and Commands

3.7.1. Static Loading Scenario

In this scenario, the mechanism is loaded with 24.5 N force to simulate suspension’s static position.

As it is presented in Figure 39, the deflection is 24.1 mm according to the FEA. Calculated value of the deflection using Eq. (3.38) was 23.1 mm. Thus, we can conclude that the amount of error is acceptable.

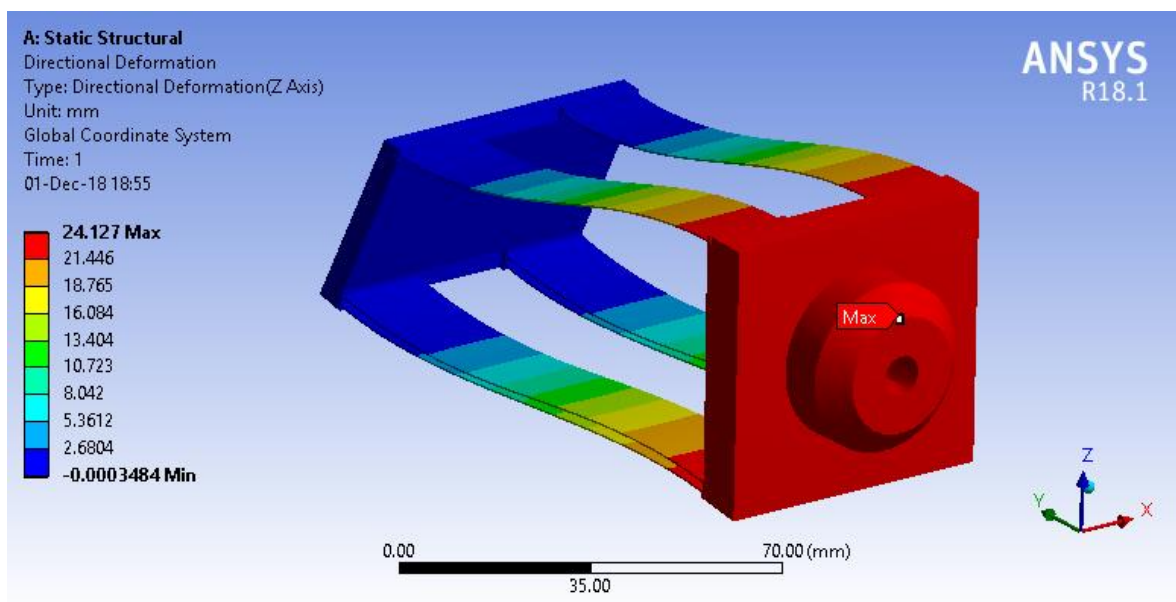


Figure 39 Static Loading Scenario, Deformation

Equivalent stress of this loading case is presented in Figure 40. Maximum stress calculated with Eq. (3.40) is 592 MPa for upper wishbone, 344 MPa for lower wishbone. Factor of safety for this loading case is 1.6.

On this load case, camber angle is also measured in Ansys using the method described in section 3.7. The change of camber angle from the mechanisms non-deflected state to its static position from analysis is 4.16°. The analytically calculated camber variation value is 3.93° (Figure 26).

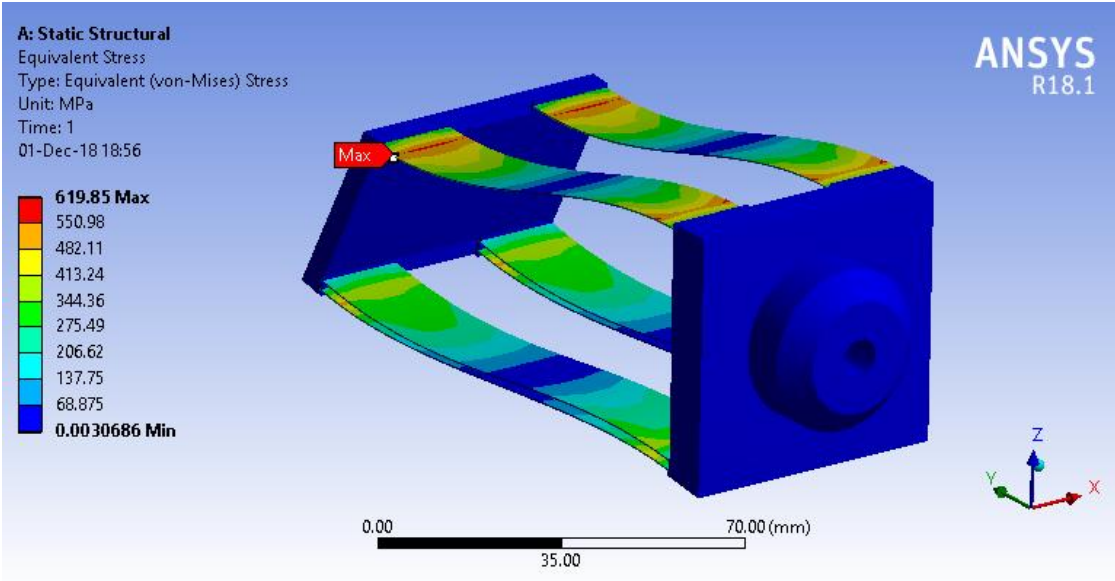


Figure 40 Static Loading Scenario, Von-Mises Stress

3.7.2. Maximum Bump Loading Scenario

In this case, the mechanism is loaded with 39.3 N force to get it to its bump position that is the maximum achievable stroke position of the suspension. This force value is calculated using the effective spring constant value from Eqn. (3.75) and the measured bump distance of the mechanism.

As it is presented in Figure 41, the deflection is 38.6 mm according to the FEA. Calculated value of the deflection using Eq. (3.38) is 37.5 mm.

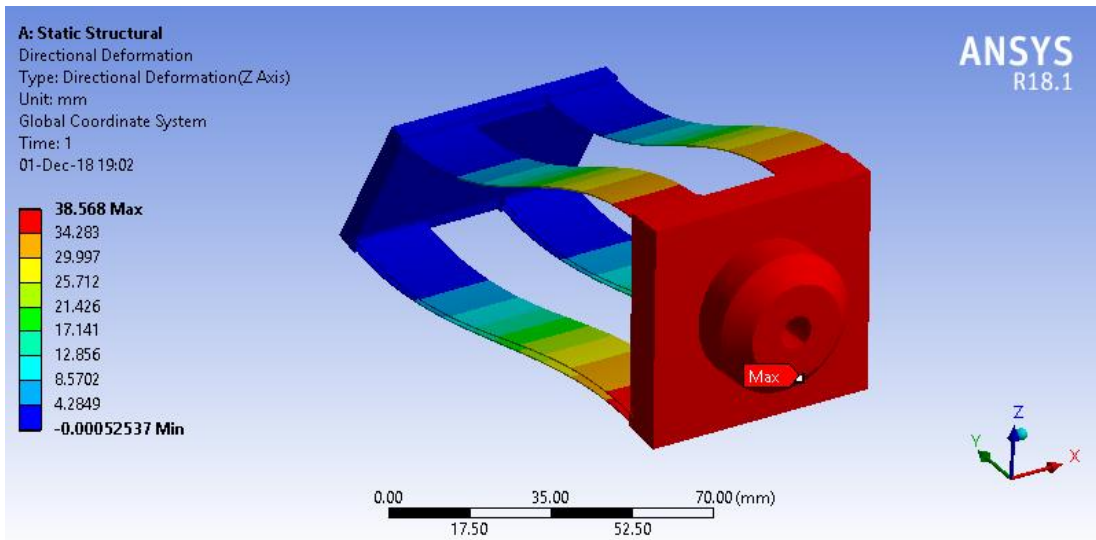


Figure 41 Maximum Bump Loading Scenario, Deformation

Equivalent stress of this load case is presented in Figure. Maximum stress calculated with Eq. (3.40) is 920 MPa for upper wishbone, 535 MPa for lower wishbone. Factor of safety for this case is almost 1 but it may be acceptable for this case because this is an extreme and unlikely case. Also, the material is not brittle, and fatigue is not an issue for this rare case. Camber variation is measured for bump load case as well. Variation of camber angle from the mechanisms non-deflected state to its bump position from analysis is 7.04° . Calculated camber variation value is 7.16° .

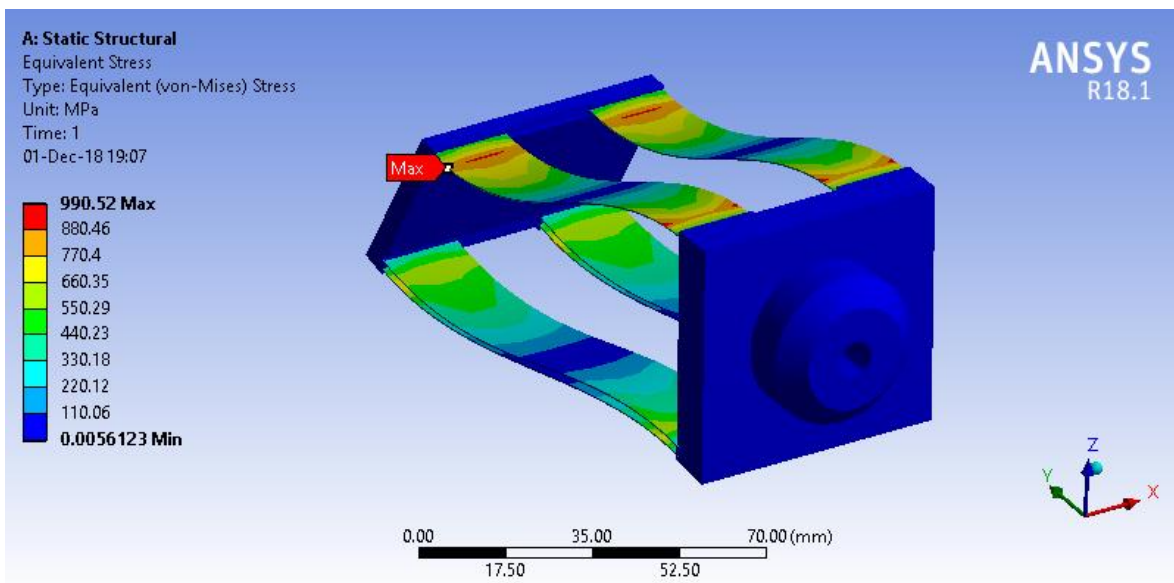


Figure 42 Maximum Bump Loading Scenario, Von-Mises Stress

3.7.3. Maximum Braking Scenario

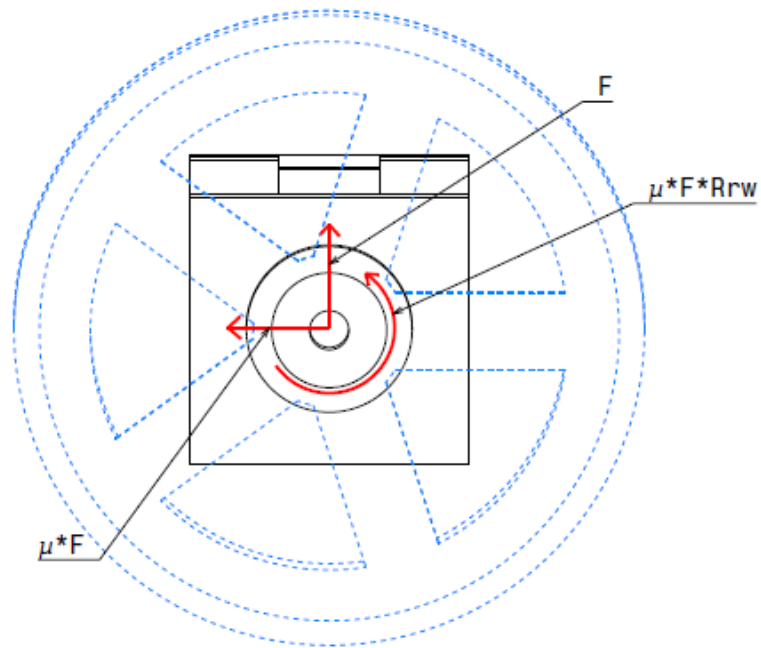


Figure 43 Maximum Braking Scenario

Braking force is applied to the system after it is in zero suspension stroke condition. As it is presented in Figure 44a plot, dashed line is the F force and it brings the mechanism to its zero stroke position and solid line is the μF force and it simulates the braking force. Same thing is applied to the braking moment applied to the mechanism on Figure 44b. On the moment plot, there is no moment applied until the mechanism is at zero stroke position.

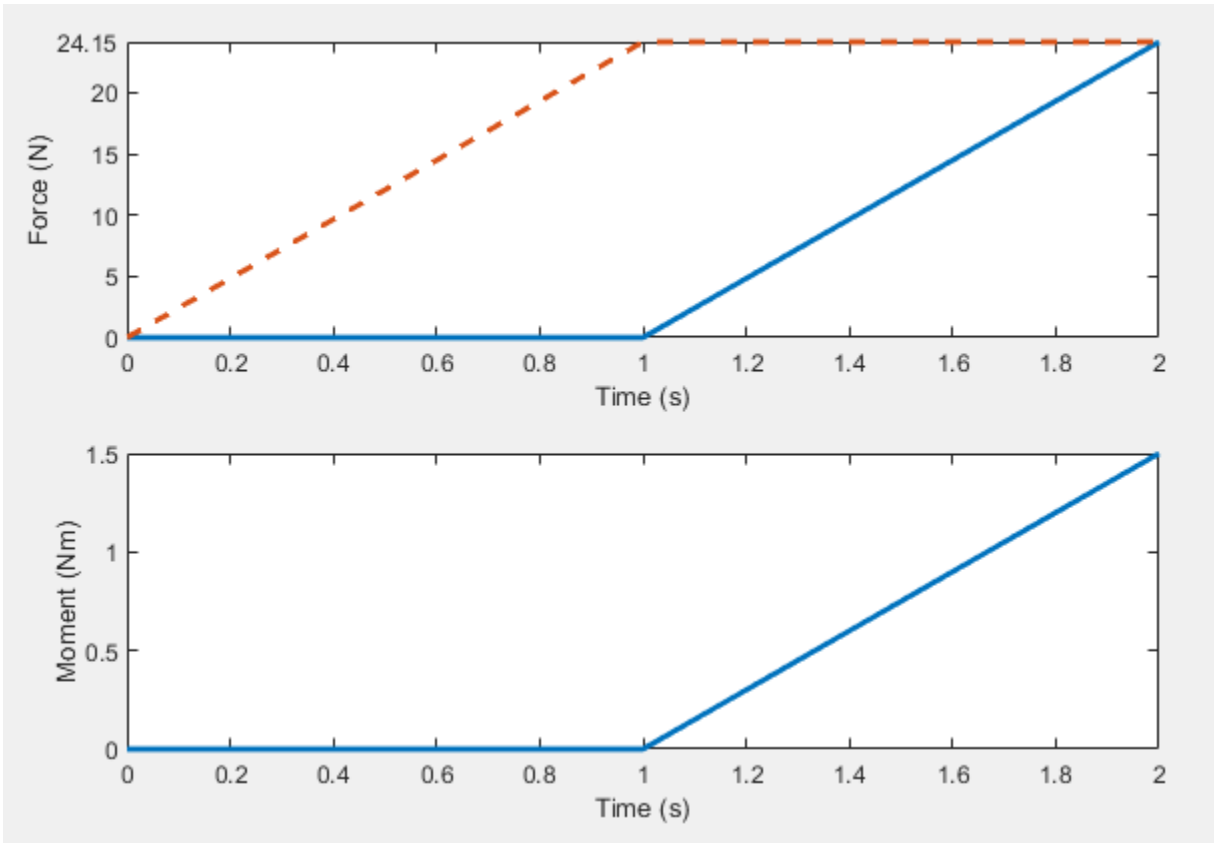


Figure 44 Maximum Braking Scenario Force (a) Moment (b) Plot

Force $\mu * F$ created by friction at the tire contact area is moved to the middle of the knuckle. Moment created because of moving the force is also added to the analysis. The deformation analysis result is presented in Figure 45. Stress analysis, presented in Figure 46, of the case yielded a 752 MPa maximum stress. Factor of safety for this case is 1.33.

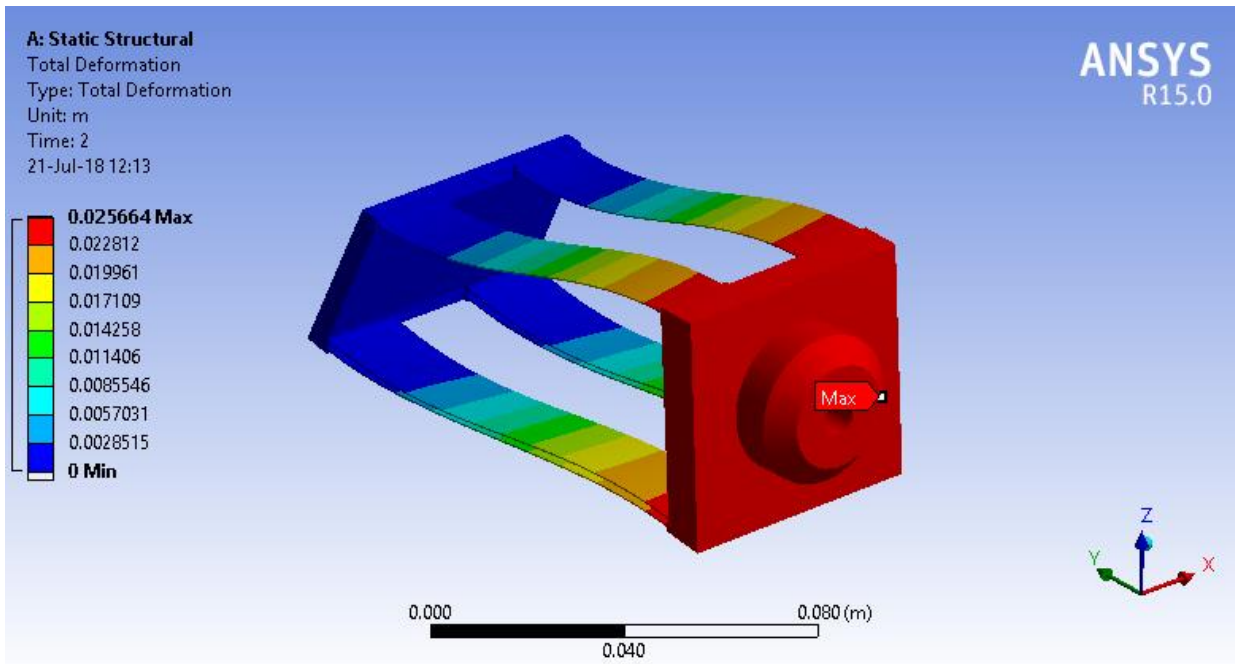


Figure 45 Maximum Braking Scenario, Deformation

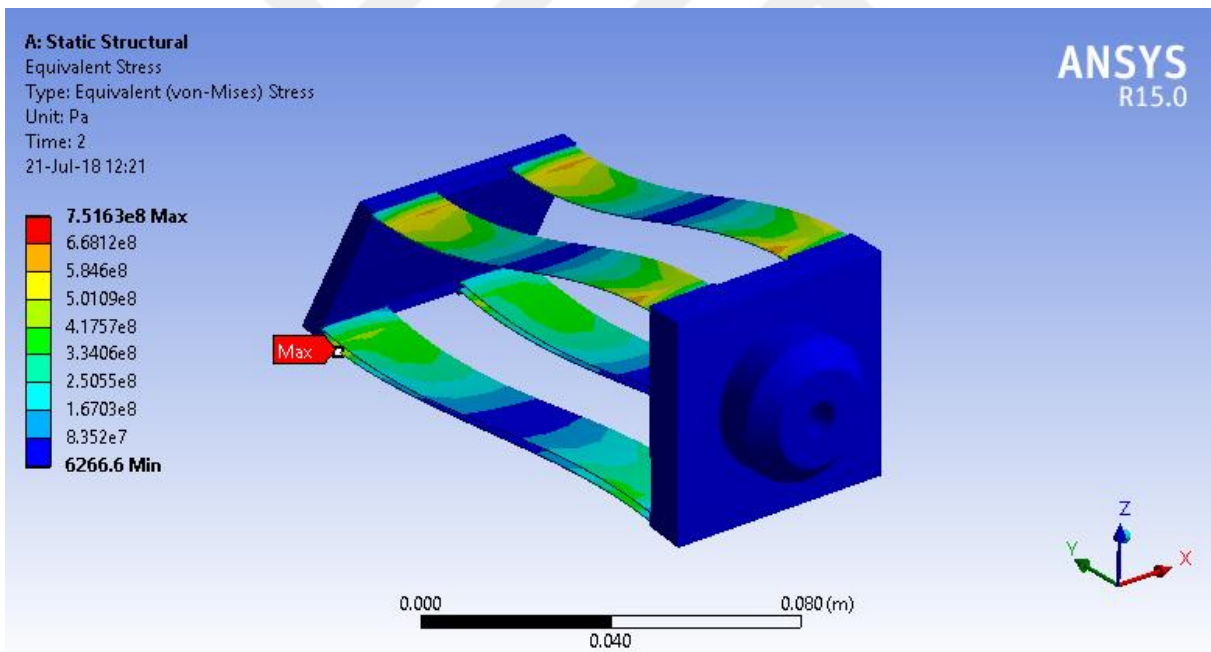


Figure 46 Maximum Braking Scenario, Von-Mises Stress

Directional deformation of the suspension system in the x axis is analyzed to calculate twist angle of the knuckle under maximum braking force. Using the ratio of differential deformation on the knuckle from Figure 47 and the height of the knuckle, maximum twist angle for the knuckle under this worst-case scenario is 1.5°. This result is acceptable, and this analysis shows that the suspension system is rigid enough around y axis. In order to

assure this rigidity, wishbones of the suspension system are designed in two parts and lower wishbones are in double layer configuration.

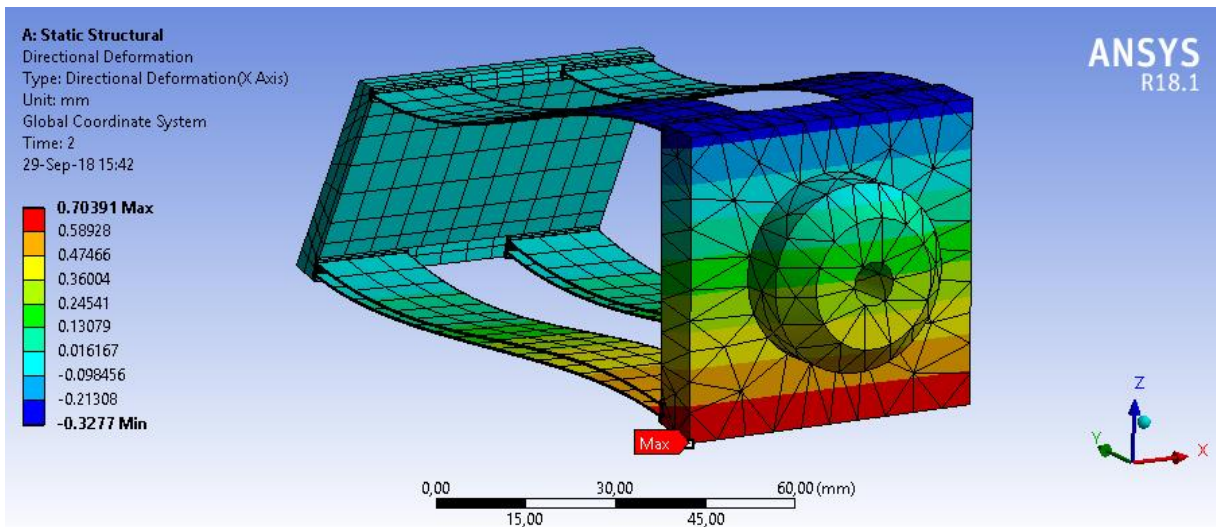


Figure 47 Maximum Braking Scenario, X Axis Directional Deformation

3.7.4. Curb Hitting Scenario

Curb hitting load case is simulated while the mechanism at zero suspension stroke.

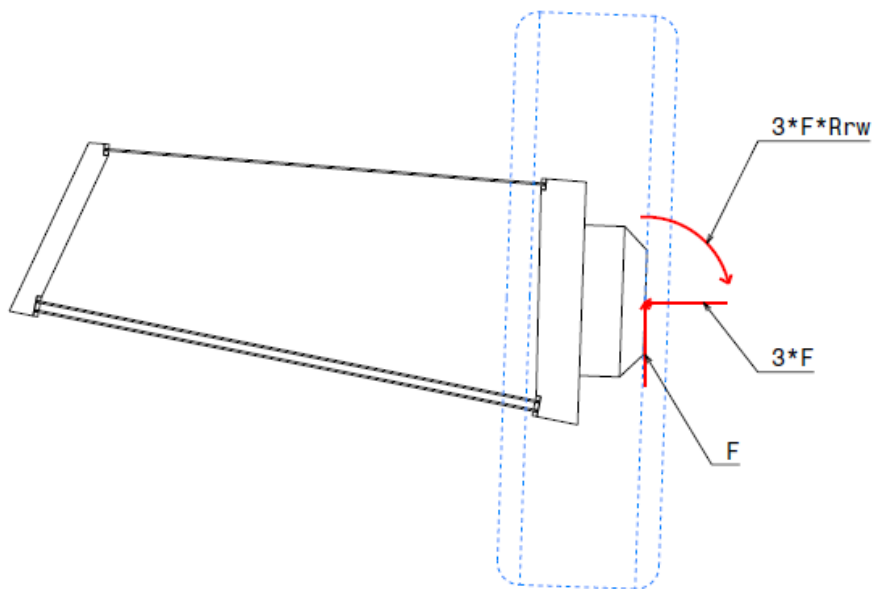


Figure 48 Curb Hitting Scenario

Force $3F$, created by the impact load because of curb hitting scenario is moved to the middle of the knuckle. Moment created because of moving the force is also added to the analysis.

Curb hitting force is applied to the system after applying the force that brings the suspension to its zero stroke. As it is presented in Figure 49a plot, dashed line is the F force and it brings the mechanism to its zero stroke position and solid line is the $3F$ force and it simulates the curb hitting force. The same approach is used to apply the bending moment to the mechanism due to hitting motion. In Figure 49b, there is no moment applied until the mechanism is at static position. This way, the case is simulated more realistically.

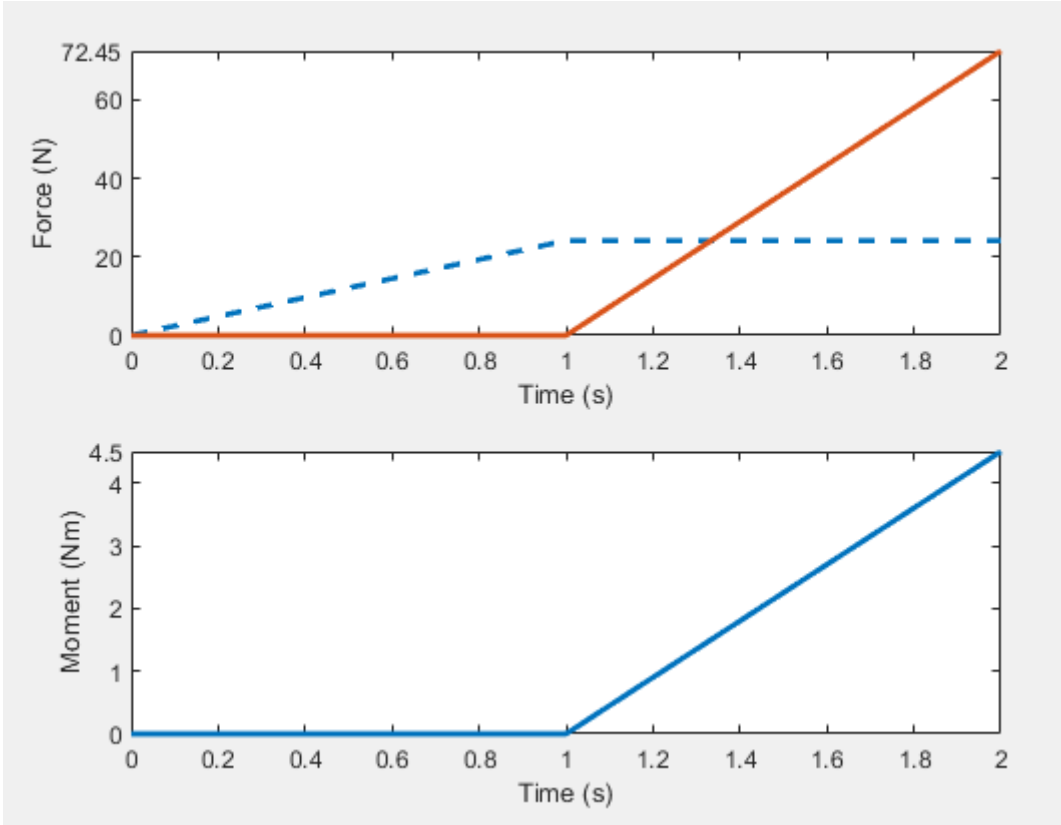


Figure 49 Curb Hitting Scenario Force (a) Moment (b) Plot

The deformation analysis result is presented in Figure 50. Stress analysis, presented in Figure 51, of the case yielded a 320 MPa maximum stress.

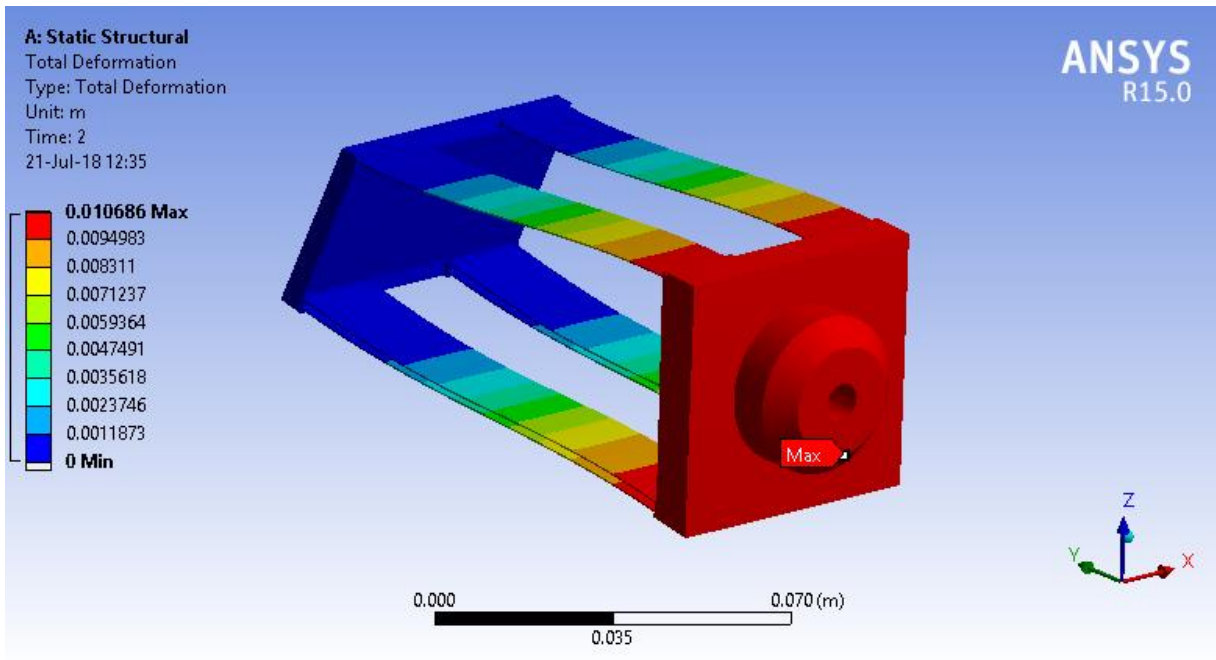


Figure 50 Curb Hitting Scenario, Deformation

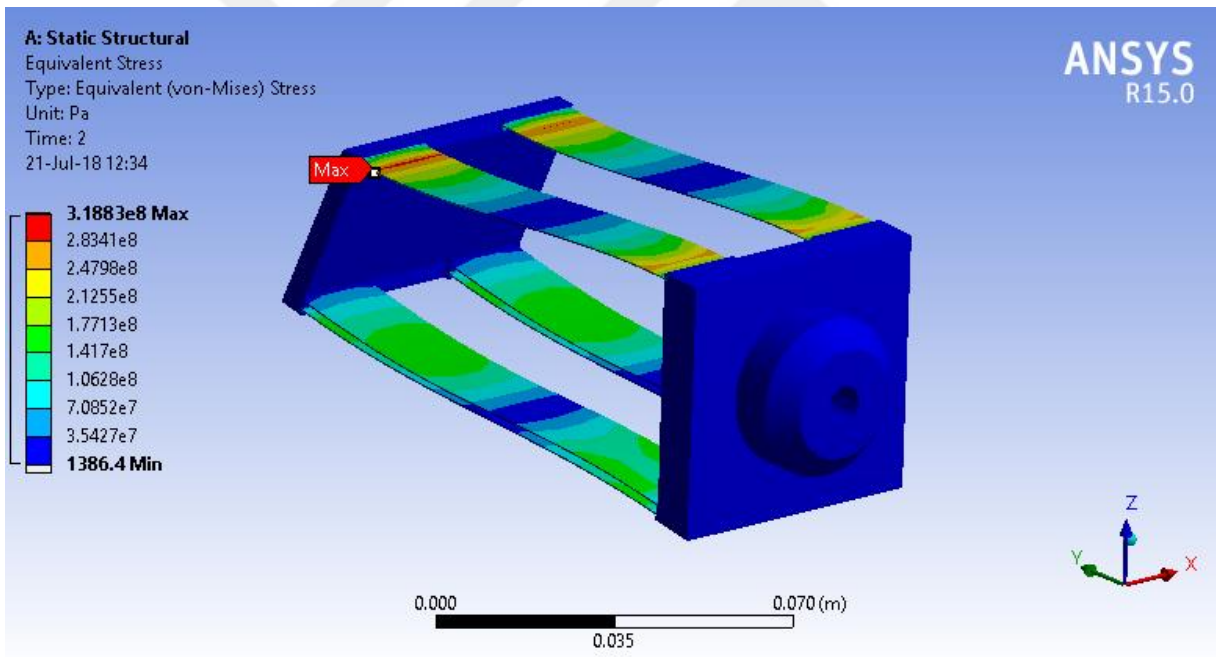
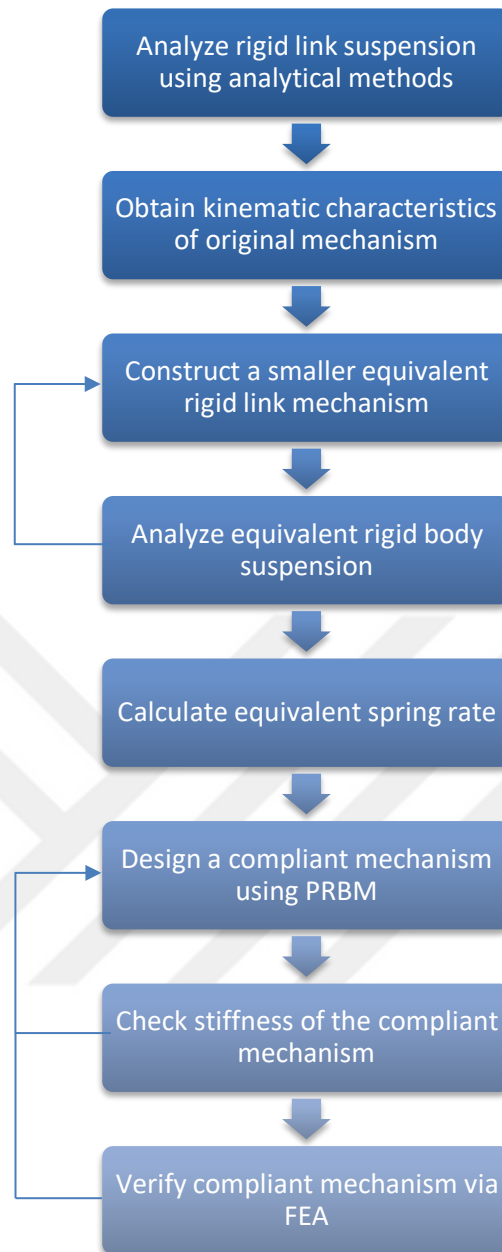


Figure 51 Curb Hitting Scenario, Von-Mises Stress

Because of the geometrical shape of the mechanism, any force applied perpendicular to the tire plane lifts the car. Because of that deflection of the mechanism decreases and stress values decrease with respect to it. Factor of safety for this case is 3.13.



Final mechanism passed from all the steps listed in above design flow chart and is therefore a suitable design.

Analysis results taken from ANSYS showed the mathematical model used to design this compliant mechanism supplies acceptable levels of error regarding deflection values. The comparison for deflection is presented in Table 8.

Table 8 FEA and Calculation Deflection Comparison Table

	Deflection (mm)		
	Calculation	FEA	Error %
Static	23.1	24.1	5.7
Bump	37.5	38.6	4.1

Comparison of FEA and calculation for stress values is presented in Table 9. These values are also acceptable, and results prove that calculation methods can be used as main design tools for appropriate compliant mechanism types.

Table 9 FEA and Calculation Von Misses Stress Comparison Table

		Von Misses Stress (MPa)		
		Calculation	FEA	Error %
Static	Upper Wishbone	592	620	4.5
	Lower Wishbone	344	380	9.5
Bump	Upper Wishbone	920	990	4.2
	Lower Wishbone	535	600	7.8

Camber variation comparison for FEA and calculation is presented in Table 10.

Table 10 FEA and Calculation Camber Comparison Table

	Camber (deg)		
	Calculation	FEA	Error %
Static	3.93	4.16	5.5
Bump	7.16	7.04	1.7

Robustness of the final compliant mechanism should be tested by manufacturing a prototype.

4. CONCLUSION

In this thesis, aim is to present a novel design methodology for a compliant suspension mechanism. Regarding this approach, a scaled car suspension mechanism was modeled in CATIA and kinematic parameters are obtained from this model. These data were used to analyze the suspension and these analyses yielded necessary motion criteria. A rigid body suspension synthesized according to these criteria and this suspension is converted to compliant suspension mechanism using pseudo rigid body model. After conversion to compliant mechanism, stiffness of the mechanism is checked. Initially, single layer of compliant segments used for both upper and lower wishbones, but this configuration resulted in very high levels of stresses in compliant segments. To reduce these stress values while keeping the mechanism geometry unchanged, lower wishbone is converted to two-layer configuration while upper wishbone is still in one layer. After this change, mechanism was performing under the materials yield strength values. This process is verified with hand calculations and finite element analysis using ANSYS.

At the end of this thesis, a suitable compliant mechanism equivalent of a rigid link mechanism is obtained. A final step or future work of verifying the robustness of the design proposed is to manufacture and test real model.

5. REFERENCES

- [1] F. Reuleaux, *The Kinematics of Machinery: Outlines of a theory of machines*, London: Macmillan and co., 1876.
- [2] G. N. Sandor and A. G. Erdman, *Advanced Mechanism Design*, Englewood Cliffs, NJ: Prentice-Hall, 1984.
- [3] V. Parlaktaş, *Mechansms Lecture Notes*, Ankara: Hacattepe University, 2013.
- [4] E. Tanık, *Design of Rigid and Compliant Mechanisms Class Notes*, Ankara: Hacettepe University, 2016.
- [5] E. Tanık and V. Parlaktaş, "On the analysis of double wishbone suspension," *Journal of Advanced Mechanical Design, Systems, and Manufacturing*, vol. 9, no. 3, pp. 1-10, 2015.
- [6] D. A. Crolla, *Powertrain, Chassis System and Vehicle Body*, Burlington: Elsevier, 2009.
- [7] T. Gillespie, *Fundamentals of Vehicle Dynamics*, Warrendale, PA: Society of Automotive Engineers, 1992.
- [8] J. C. Dixon, *Suspension Geometry and computation*, West Sussex: John Wiley & Sons, 2009.
- [9] J. Dixon, *Tires, Suspension and Handling*, Warrendale, PA: Society of Automotive Engineers, 1996.
- [10] V. Parlaktaş and E. Tanık, "Partially compliant spatial slider–crank (RSSP) mechanism," *Mechanism and Machine Theory*, vol. 46, no. 11, pp. 1707-1718, 2011.
- [11] L. L. Howell, *Compliant Mechanisms*, New York: John Wiley & Sons Ltd., 2001.
- [12] T. M. Allred, "Compliant Mechanism Suspensions," Brigham Young University, Utah, 2006.
- [13] Ç. M. Tanık, V. Parlaktaş and E. Tanık, "Steel Compliant Cardan Universal Joint," *Mechanism and Machine Theory*, no. 92, pp. 171-183, 2015.
- [14] H. A. Schmid, J. P. Ryan and S. P. Fuja, "Design Synthesis of Suspension," no. SAE Paper no. 970092, 1997.
- [15] J. Reimpell and H. Stoll, *The Automotive Chassis: Engineering Principles*, Würzburg: Vogel-Buchverlag, 1998.

- [16] E. Tank and V. Parlaktaş, "Design of a Very Light L7e Electric Vehicle Prototype," *International Journal of Automotive Technology*, vol. 16, no. 6, pp. 997-1005, 2015.
- [17] D. Bastow and G. Howard, *Car Suspension and Handling*, London: Pentech Press Limited, 1993.





HACETTEPE UNIVERSITY
GRADUATE SCHOOL OF SCIENCE AND ENGINEERING
THESIS/DISSERTATION ORIGINALITY REPORT

HACETTEPE UNIVERSITY
GRADUATE SCHOOL OF SCIENCE AND ENGINEERING
TO THE DEPARTMENT OF MECHANICAL ENGINEERING

Date: 25/02/2019

Thesis Title / Topic: A COMPLIANT SUSPENSION APPLICATION TO A SMALL SCALE CAR

According to the originality report obtained by myself/my thesis advisor by using the Turnitin plagiarism detection software and by applying the filtering options stated below on 20/02/2019 for the total of 50 pages including the a) Title Page, b) Introduction, c) Main Chapters, d) Conclusion sections of my thesis entitled as above, the similarity index of my thesis is 10 %.

Filtering options applied:

1. Bibliography/Works Cited excluded
2. Quotes excluded /-included-
3. Match size up to 5 words excluded

I declare that I have carefully read Hacettepe University Graduate School of Science and Engineering Guidelines for Obtaining and Using Thesis Originality Reports; that according to the maximum similarity index values specified in the Guidelines, my thesis does not include any form of plagiarism; that in any future detection of possible infringement of the regulations I accept all legal responsibility; and that all the information I have provided is correct to the best of my knowledge.

I respectfully submit this for approval.


Name Surname: Çağrı Bekir Baysal

Student No: N14325296

Department: Mechanical Engineering

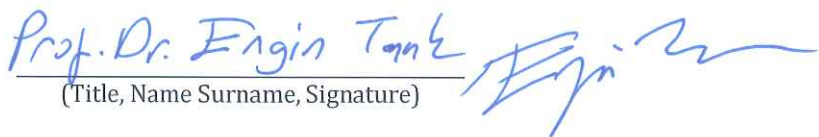
Program: -

Status: Masters Ph.D. Integrated Ph.D.


Date and Signature
25.02.2019

ADVISOR APPROVAL

APPROVED.


(Title, Name Surname, Signature)

ÖZGEÇMİŞ

Adı Soyadı : Çağrı Bekir Baysal
Doğum yeri : Elazığ / Merkez
Doğum tarihi : 09 / 09 / 1992
Medeni hali : Bekar
Yazışma adresi : Topçu Mah. 1497. Sk. 6/6 Etimesgut / Ankara
Telefon : 05066800068
Elektronik posta adresi : cbekirb@gmail.com
Yabancı dili : İngilizce

EĞİTİM DURUMU

Lisans : Hacettepe Üniversitesi Makina Mühendisliği
Yüksek Lisans : -
Doktora : -

İş Tecrübesi

2014 – 2015	EVT Motor	Part Time Mühendis
2015 – 2016	EVT Motor	Mekanik Tasarım Mühendisi
2016 –	Nurol Makina	Mekanik Tasarım Mühendisi